J. Fluid Mech. (1986), *vol.* 171, *pp.* 145–181
Printed in Great Britain

Self-accelerating turbidity currents

By GARY PARKER,

St Anthony Falls, Hydraulic Laboratory, University of Minnesota, Minneapolis, Minnesota 55414, USA

YUSUKE FUKUSHIMA

Faculty of Engineering, Technological University of Nagaoka, Niigata, Japan

AND HENRY M. PANTIN

British Geological Survey, Keyworth, Nottingham NG12 5GG UK

(Received 25 May 1984 and in revised form 24 March 1986)

Approximate layer-averaged equations describing the mechanics of turbid underflows are derived. Closure of the equations describing the balance of fluid mass, sediment mass, and mean flow momentum provides for the delineation of a three-equation model. A description of sediment exchange with the bed allows for the possibility of a self-accelerating turbidity current in which sediment entrainment from the bed is linked to flow velocity. A consideration of the balance of the mean energy of the turbulence yields a constraint on physically realistic solutions to the three-equation model. It is shown that the self-acceleration predicted by the three-equation model is so strong that the energy constraint fails to be satisfied. In particular, the turbulent energy consumed in entraining new bed sediment exceeds the supply of energy to the turbulence, so that the turbulence, and thus the turbidity current, must die. The problem is rectified by the formulation of a four-equation model, in which an explicit accounting is made of the mean energy of the turbulence. Sediment entrainment from the bed is linked to the level of turbulence in the four-equation model. Self-acceleration is again predicted, although it is somewhat subdued compared with that predicted by the three-equation model. The predictions of both models are summarized over a wide range of conditions.

1. Introduction

Turbidity currents are sediment-laden underflows that occur in the ocean and lakes. They constitute an important mechanism for the transport of littoral sediment to deeper waters. In the process of doing so, they have scoured out many (but not all) subaqueous canyons.

It has become apparent that turbidity currents in submarine canyons can attain surprisingly swift velocities, as high as 8–14 m/s (e.g. Krause *et al.* 1970). The generation of such high velocities in otherwise still water constitutes a most intriguing problem. High velocity is presumably attained as the result of acceleration from some lower velocity constituting an initial perturbation. In particular, one may speculate that in the absence of such topographic changes as a submerged overfall or an increase in canyon-bed slope in the down-canyon direction, the energy for acceleration must be derived from the sediment itself.

The energy of a true turbidity current is obtained from the work performed by the downstream component of gravity on the suspended sediment, that is, the sediment

drags the water along (Bagnold 1962). It is helpful to consider a submarine canyon, the bed of which is covered by a plethora of loose sand of similar composition to the sand suspended in a turbidity current flowing over it. If the current is sufficiently swift, it may entrain even more sediment from the bed, thus increasing the rate of work performed by gravity. As a result, the current may accelerate, thus entraining even more bed sediment, in a self-reinforcing cycle.

The only case for which this process has been observed in any detail is that of Scripps Submarine Canyon (Inman, Nordstrom & Flick 1976). Sand is delivered to the head of the canyon by littoral drift. During storms, a pattern of edge waves is set up along the shore, with an antinode at the head of the canyon. The waves act to stir up sand at the head and to induce a weak, oscillating down-canyon flow, with peak velocities as high as 50 cm/s. Initially, discontinuous turbidity currents peel off from the head region at intervals; these dissipate and deposit the sand farther down-canyon. If a storm is of sufficient intensity and duration, however, continuous, sustained turbidity currents are generated. These develop and accelerate in the downstream direction. Velocities as high as 1.9 m/s have been measured not far downstream of the head, and Inman *et al.* (1976) cite circumstantial evidence for much higher velocities farther downstream.

Many attempts have been made to delineate the governing layer-averaged equations of motion for density underflows in general, and turbidity currents in particular (e.g. Ellison & Turner 1959; Hinze 1960; Plapp & Mitchell 1960; Chu, Pilkey & Pilkey 1979; Lüthi 1981). Turbidity currents differ from the simple, conservative density underflows studied by Ellison & Turner (1959) in that the source of the buoyancy difference, i.e. the suspended sediment, is not conserved; suspended sediment is free to exchange with bed sediment. This exchange was quantified in terms of bed erosion and deposition by Pantin (1979) and Parker (1982). Both Pantin and Parker found that this additional degree of freedom allows for the possibility of self-acceleration via the entrainment of bed sediment; Parker called the phenomenon 'ignition'.

The analyses of Pantin and Parker are both concerned with a simple conceptual model, i.e. a continuous, spatially uniform flow that is free to change in time. The entrainment of sediment from the bed, and deposition thereon, is allowed, but water entrainment into the current from above is taken to be negligible. In the light of the results of Inman *et al.* (1976), however, a more realistic conceptual model consists of a steady flow developing in the downstream direction, free to exchange sediment with the bed and entrain water from above.

Such a model is pursued herein, in terms of a closed set of layer-averaged equations of motion for the flow. In fact two models are derived herein; they are called the three-equation model and the four-equation model. The difference between the two is that the former does not include an equation of balance for the mean energy of the turbulence, whereas the latter does. The latter is necessitated by the breakdown of the former under conditions of severe acceleration. Calculations specifically for the case of Scripps Submarine Canyon are presented in Fukushima, Parker & Pantin (1985).

2. The layer-averaged equations of motion

A complete derivation of the layer-averaged equations of motion can be found in the Appendix to this paper. Herein the results of that analysis are summarized.

A dilute turbidity current in a wide submarine canyon with constant down-canyon

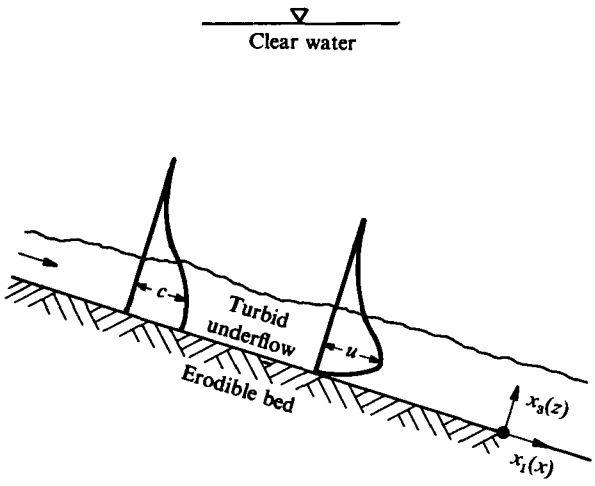

FIGURE 1. Definition diagram, wherein u is velocity and c is volumetric concentration of sediment; x_1 and x_3 are reference axes.

slope is considered. As shown in figure 1, the flow is taken to be essentially two-dimensional. The turbidity current carries uniform non-cohesive sediment with fall velocity v_s, which is free to exchange with similar sediment on the canyon bed. In the Appendix certain constraints and approximations are imposed to allow for the derivation of layer-averaged equations of motion for non-conservative turbid underflows. The important layer-averaged quantities are flow velocity U, volumetric concentration of suspended sediment C, layer thickness h, and level of turbulence (mean turbulent kinetic energy per unit mass) K. Some auxiliary parameters are the velocity of entrainment w_e of clear water from above, the near-bed volumetric sediment concentration (averaged over turbulence) c_b, the bed shear velocity u_*, and the vertical volumetric Reynolds flux of suspended sediment F, where

$$F = \overline{c'w'} \tag{1}$$

as defined in (A 19). Note that the value of F near the bed is denoted F_b. and is quantified in terms of a dimensionless coefficient of bed sediment entrainment E_s, where

$$v_s E_s = F_b. \tag{2}$$

The layer-averaged equations of balance of fluid mass, sediment mass, and momentum, (A 37), (A 43), and (A 44) can be cast in the respective forms

$$\frac{\partial h}{\partial t} + \frac{\partial Uh}{\partial x} = e_w U, \tag{3}$$

$$\frac{\partial Ch}{\partial t} + \frac{\partial UCh}{\partial x} = v_s(E_s - r_0 C), \tag{4}$$

$$\frac{\partial Uh}{\partial t} + \frac{\partial U^2 h}{\partial x} = -\tfrac{1}{2}Rg\frac{\partial Ch^2}{\partial x} + RgChS - u_*^2, \tag{5}$$

where

$$r_0 = \frac{c_b}{C} \tag{6}$$

and the coefficient of water entrainment from above is given by

$$e_w = \frac{w_e}{U}. \tag{7}$$

Also, R denotes the submerged specific gravity of the sediment; it is taken to be equal to the value for quartz, 1.65, herein.

The mechanism for self-acceleration is intimately associated with the right-hand side of (4), which can be written with the aid of (6) as $v_s(E_s - c_b)$. If E_s exceeds c_b, the current entrains more sediment than it loses through deposition. As a result, the current may become heavier, increasing the term $RgChS$ that quantifies the driving force of the current in (5). As a result the current may accelerate. The increase in U can be expected to increase the sediment entrainment rate $v_s E_s$ in a self-reinforcing cycle. It is the nature of this mass–momentum interaction that is the topic of the present paper.

Turbulent energy is expended, however, in both maintaining the existing load in suspension, and entraining new sediment from the bed. An arbitrarily large rate of entrainment of sediment from the bed cannot be maintained because the rate of expenditure of turbulent energy may exceed the supply from the mean flow. This would eventually cause the turbulence to collapse, the sediment held in suspension to settle out, and the current to die. Such an energy constraint can best be quantified in terms of the layer-averaged equation of balance of turbulent kinetic energy (A 46). When reduced with the aid of (A 48), (6) and (7), it takes the form

$$\frac{\partial Kh}{\partial t} + \frac{\partial UKh}{\partial x} = u_*^2 U + \tfrac{1}{2}U^3 e_w - \epsilon_0 h - Rgv_s Ch - \tfrac{1}{2}RgChUe_w - \tfrac{1}{2}Rghv_s(E_s - r_0 C). \tag{8}$$

The first two terms on the right-hand side of (8) quantify the rate of production of turbulent energy. In the next term, ϵ_0 denotes the layer-averaged mean rate of dissipation of turbulent energy due to viscosity. The final three terms represent the rate of turbulent energy expenditure due to working against the density gradient. These three final terms can be simply related to the buoyancy flux, given by RgF; it can be shown from (A 14) and (A 23), and the general assumptions of the Appendix, that

$$Rg\int_0^\infty F\,\mathrm{d}z = Rgv_s Ch + \tfrac{1}{2}RgChw_e + \tfrac{1}{2}Rghv_s(E_s - c_b), \tag{9}$$

that is the three terms on the right-hand side of the above equation, which are also the three final terms on the right-hand side of (8), quantify the effect of sediment-induced stratification.

3. A generalized Knapp–Bagnold constraint

The first term on the right-hand side of (9) is the Knapp–Bagnold term (Knapp 1938; Bagnold 1962). It represents the work necessary to maintain a given suspension in equilibrium, so as to prevent the sediment from falling out. The second term pertains to a layer that thickens by the entrainment of water from above, as illustrated in figure 2. As the layer thickens, turbulence acts to raise the centre of gravity, and thus the potential energy of the suspension, expending kinetic energy in the process. In the present simplified treatment, the centre of gravity of the suspension is at $\frac{1}{2}h$, and the rate of increase of thickness of the suspension layer due to water entrainment from above is w_e. The final term, illustrated in figure 3, likewise

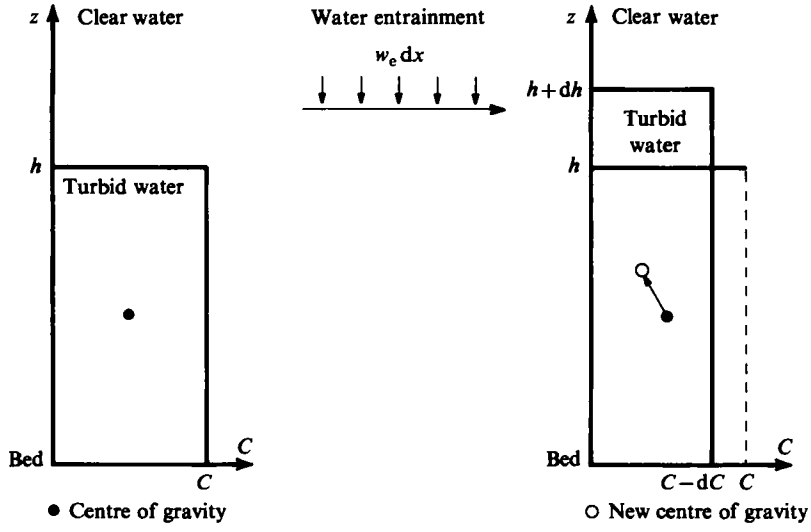

FIGURE 2. Illustration of the effect of water entrainment from above on the sediment. For simplicity, a vertically uniform current with concentration C and height h is considered. As water is entrained and mixed by turbulence into the suspension, the centre of gravity rises. The resulting increase in the potential energy of the suspension is thus obtained at the expense of a loss of the turbulent kinetic energy that accomplished the mixing.

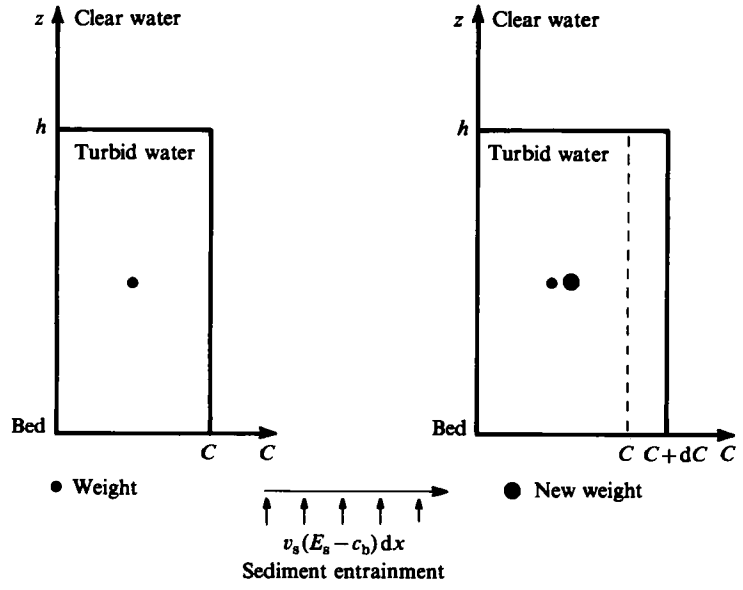

FIGURE 3. Illustration of the effect of sediment entrainment from the bed on energy balance. The case for which $E_s > c_b$ is considered. As sediment is entrained from the bed, it is mixed by turbulence throughout the suspension. As a result, the weight of the suspension per unit area, and thus its potential energy, increases. This increase is again obtained at the expense of the turbulent kinetic energy that accomplished the mixing.

quantifies the energy expended in lifting up newly entrained sediment and incorporating it into the suspension (at an average elevation of $\frac{1}{2}h$ above the bed). The term can be positive (representing a kinetic energy loss) or negative (representing a kinetic energy gain), depending upon whether or not the entrainment rate of sediment from the bed $v_s E_s$ exceeds the deposition rate $v_s c_b$.

An important parameter governing the behaviour of stratified, slender flows is the Richardson number

$$Ri = \frac{RgCh}{U^2}. \tag{10}$$

If the Richardson number exceeds a critical value near unity, the flow is termed subcritical. The entrainment of water from above becomes small, and w_e can be taken to vanish (Turner 1973). Under these constraints, (3), (4), (5) and (8) possess equilibrium solutions with constant values of U, C, h and K. From (5), the momentum balance is

$$u_*^2 = RgChS. \tag{11}$$

From (4), the sediment mass balance reduces with the aid of (6) to

$$E_s = c_b. \tag{12}$$

From (8), (A 47), (A 48), (11) and (12), the energy balance of the turbulence is thus

$$u_*^2 U = RgChUS = \epsilon_0 h + Rgv_s Ch. \tag{13}$$

Equation (13) has a simple interpretation. For turbid underflows of the type illustrated in the figure, gravity does no work on the fluid phase. The term $RgChUS$ represents the power supplied to the flow by the action of the down-slope component of gravity on the suspended sediment. This energy must be expended in working against the vertical pull of gravity in order to hold the sediment in suspension, and in viscous dissipation. It is seen from (A 22) that ϵ, and thus its layer average ϵ_0, is a non-negative quantity. It follows from (13) that a necessary condition for an equilibrium, self-sustaining turbid underflow of constant thickness is the condition

$$u_*^2 U = RgChUS > Rgv_s Ch, \tag{14a}$$

or

$$\frac{US}{v_s} > 1. \tag{14b}$$

Equation (14b) is the Knapp–Bagnold criterion. Knapp (1938) and Bagnold (1962) argued further that if it is satisfied, the concentration, and thus the velocity of the turbidity current might rise indefinitely because according to (14a) more energy is fed in via the sediment than is consumed in holding it in suspension.

The criterion (14b), however, is not in fact sufficient for either an equilibrium or an accelerating turbidity current, as Parker (1982) indicated. Indeed, (14b) must be generalized as even a necessary condition if it is to be applied to the supercritical ($Ri < 1$) disequilibrium currents studied herein.

Equation (8) can be recast in the form

$$\frac{\partial K}{\partial t} + U\frac{\partial K}{\partial x} = \frac{u_*^2 U + \frac{1}{2}U^3 e_w}{h} - \epsilon_0 - Rg[v_s C + \tfrac{1}{2}e_w UC + \tfrac{1}{2}v_s(E_s - r_0 C)] - e_w \frac{K}{h} U. \tag{15}$$

It follows, then, that if the inequality

$$u_*^2 U + \tfrac{1}{2}U^3 e_w > Rgh[v_s C + \tfrac{1}{2}e_w UC + \tfrac{1}{2}v_s(E_s - r_0 C)] \tag{16}$$

fails to be satisfied over a sufficiently long reach or flow a sufficiently long time, the turbulence must die. As a consequence, all the sediment would settle out, and the current itself would die.

It should be emphasized that criterion (16) puts limits on, rather than makes possible, self-acceleration. In particular, it will be shown that sustained accelerating flows with large sediment entrainment rates (large E_s) are not physically possible, even though they satisfy mass and momentum balance; such flows consume more turbulent energy in suspending new sediment than is available from the flow.

4. Steady flows developing in the downstream direction

As noted in the Introduction, steady flows developing in the downstream direction are considered herein. Under this constraint (3), (4), (5) and (8) can be cast in the respective forms

$$\frac{\mathrm{d}h}{\mathrm{d}x} = \frac{-RiS + e_w(2-\frac{1}{2}Ri) + \frac{u_*^2}{U^2} + \frac{1}{2}\frac{v_s}{U} r_0 Ri\left(\frac{\psi_e}{\psi} - 1\right)}{(1-Ri)}, \tag{17a}$$

$$\frac{h}{\psi}\frac{\mathrm{d}\psi}{\mathrm{d}x} = \frac{v_s}{U} r_0 \left(\frac{\psi_e}{\psi} - 1\right), \tag{17b}$$

$$\frac{h}{U}\frac{\mathrm{d}U}{\mathrm{d}x} = \frac{RiS - e_w(1+\frac{1}{2}Ri) - \frac{u_*^2}{U^2} - \frac{1}{2}\frac{v_s}{U} r_0 Ri\left(\frac{\psi_e}{\psi} - 1\right)}{(1-Ri)}, \tag{17c}$$

$$\frac{h}{U^2}\frac{\mathrm{d}K}{\mathrm{d}x} = \tfrac{1}{2}e_w(1-Ri) + \frac{u_*^2}{U^2} - e_w\frac{K}{U^2} - \frac{\epsilon_0 h}{U^3} - Ri\frac{v_s}{U} - \frac{1}{2}\frac{v_s}{U} r_0 Ri\left(\frac{\psi_e}{\psi} - 1\right). \tag{17d}$$

In the above equations $\psi = UCh$ denotes the volumetric suspended-sediment transport rate per unit width, and

$$\psi_e = \frac{E_s h U}{r_0} \tag{18}$$

denotes the equilibrium value of ψ at which neither erosion nor deposition would occur, as can be seen from (6), (12) and (17*b*).

It is of interest to note that for the case of a simple conservative density current, for which $v_s = 0$, (17*a–c*) reduce (for order-one shape factors) to the relations of Ellison & Turner (1959).

5. Closure for the three-equation model

The simplest tenable model of eroding and depositing turbidity currents consists of the balance equations of fluid mass, sediment mass and momentum, herein termed the three-equation model. This format has been employed for the analysis of both conservative and non-conservative density flows, e.g. Ellison & Turner (1959) and Longuet-Higgins & Turner (1974). The models of Pantin (1979) and Parker (1982) of non-conservative turbidity currents are also of this type, although e_w is taken to vanish in both models, and momentum balance is replaced with overall energy balance in the model of Parker (1982).

Assumptions for the water entrainment coefficient e_w, sediment entrainment

coefficient E_s, shear velocity u_*, and concentration ratio r_0 are required to close the set (17*a–c*). The relation for water entrainment is taken to be

$$e_w(Ri) = \frac{0.00153}{0.0204 + Ri}. \tag{19}$$

According to (19), as Ri approaches zero, e_w approaches a value of 0.075, appropriate for non-stratified flows. As Ri becomes much larger than 0.0204, the formula of Egashira (1980), extensively supported by data for density-driven flows, is obtained.

Owing to the lack of information pertaining to turbidity currents from which a functional form for r_0 could be determined, recourse was made to open-channel suspensions, for which the Rousean distribution has been found to apply. Evaluating c_b at $z = b = 0.05h$, where h denotes open-channel depth in this case, Parker (1982) obtained the following approximate form:

$$r_0 = 1 + 31.5\mu^{-1.46}, \tag{20}$$

where

$$\mu = \frac{u_*}{v_s}. \tag{21}$$

Recently Garcia (1985) has tested this formula for three sets of laboratory turbidity currents, as shown in figure 4(*a*). For the range $5 < u_*/v_s < 50$ the agreement is acceptable, although a constant value of r_0 of about 1.6 would also approximate the data well.

Akiyama & Fukushima (1985) used data for open-channel suspensions in flumes and rivers to determine the following relation for E_s:

$$E_s = \begin{cases} 0.3, & Z > Z_m, \\ 3 \times 10^{-12} & Z^{10}\left(1 - \dfrac{Z_c}{Z}\right), \quad Z_c < Z < Z_m, \\ 0, & Z < Z_c, \end{cases} \tag{22}$$

where

$$Z = R_p^{0.5}\mu \tag{23}$$

and the particle Reynolds number

$$R_p = \frac{(RgD_s)^{\frac{1}{2}} D_s}{\nu}. \tag{24}$$

In (24), ν denotes the kinematic viscosity of clear water, and D_s denotes grain diameter. In (22), Z_c is a critical value for the onset of significant suspension, approximately equal to five, and the value $Z_m = 13.2$ denotes a maximum value of Z beyond which E_s becomes constant with a value of about 0.3. The data used in deriving the relationship were determined for grain diameters in the 0.06–1.00 mm range. Equation (22), although determined from open-channel suspensions, has been applied herein to turbidity currents, since direct information concerning E_s was lacking for underflows. Garcia's (1985) recent work has allowed for a test of this relationship for a set of experimental turbidity currents. Although the scatter is large, mostly owing to experimental technique, the data from turbidity currents seem to follow the trend of the flume data analysed by Akiyama & Fukushima (1985), as shown in figure 4(*b*).

Finally, the relation for bed stress is taken to be

$$u_*^2 = c_D U^2, \tag{25}$$

where c_D is a coefficient of bed drag. In general, c_D can be expected to be a function of boundary-layer parameters; herein it is approximated as constant in time or in the downstream direction for a given current.

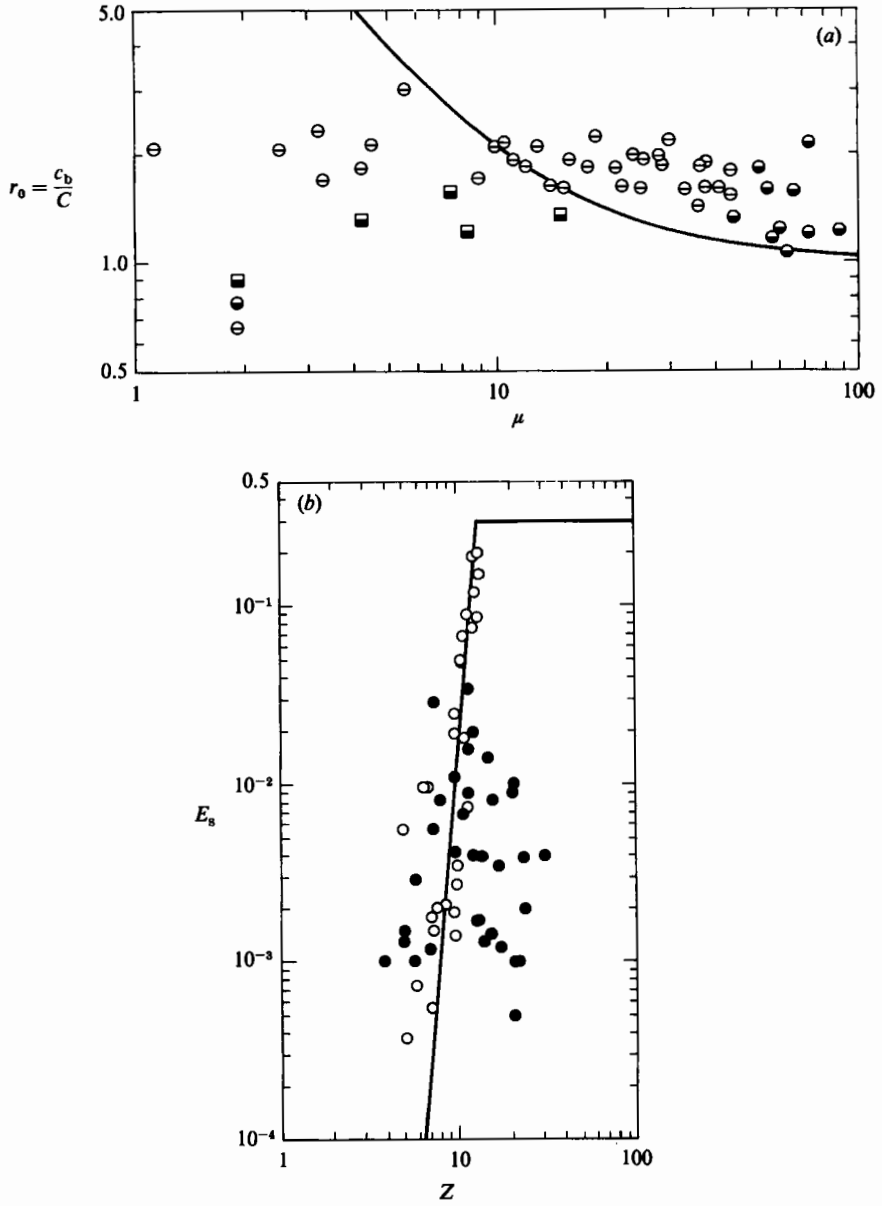

FIGURE 4. (*a*) Comparison of (20) with laboratory data for turbidity currents: ⬓, Michon, Goddet & Bonnefille (1955); ◒, Tesaker (1969); ⊖, Garcia (1985). (*b*) Comparison of (22) with laboratory data for open-channel flumes (○) and turbidity currents (●).

6. Computations with the three-equation model; breakdown of the model

Equations (17*a–c*) are to be solved downstream of the canyon head, at which the upstream values U_0, ψ_0 and h_0 are specified. It is possible to integrate (17*a–c*) downstream of a source only for the case of supercritical currents ($Ri < 1$).

In the case of simple, conservative density currents ($v_s = 0$ in the context of the present models), equilibrium solutions exist such that the right-hand sides of (17*b*) and (17*c*) vanish. These solutions are characterized by a constant Richardson

number Ri, constant values of U and ψ and a layer thickness h that increases linearly in the downstream direction (e.g. Ellison & Turner 1959).

No such equilibrium solutions exist for turbidity currents ($v_s \neq 0$). Nevertheless, for a given value of upstream layer thickness h_0, a pseudoequilibrium can be defined by setting equal to zero the right-hand sides of (17*b*, *c*) at $x = 0$. The lowest finite values of U and ψ so found are denoted as U_I and ψ_I and are said to describe the ignitive state (Parker 1982). The ignitive concentration C_I is found from the relation

$$\psi_I = U_I C_I h_0.$$

Even though the ignitive state does not constitute a true equilibrium for the currents studied herein, it will nevertheless be shown to provide a useful indicator of whether or not a current with given upstream conditions eventually accelerates or subsides.

According to (17*b*, *c*), and the closure hypotheses of the previous section, the ignition values U_I and ψ_I of the three-equation model can be computed uniquely if the dimensionless numbers S, c_D, h_0/D_s and the particle Reynolds number R_p, defined by (24), are specified. R_p is used to compute the fall velocity v_s from the drag curve for spheres (e.g. Parker 1978). For simplicity herein, the value of v for clear water at 20 °C is used, so that grain size D_s can be used as a surrogate for R_p.

A perusal of the literature (Komar 1977; Inman *et al.* 1976; Shepard & Dill 1966) suggested that the following values might be typical of sand submarine canyons likely to serve as conduits for turbidity currents: $D_s = 0.1$ mm; $S = 0.05$; $c_D = 0.004$; $h_0 = 2$ m. Values of U_I, C_I, ψ_I and the Richardson number at ignition $Ri_I = RgC_I h_0/U_I^2$, computed from the three-equation model with the above values, are shown in table 1. It is seen from the value of C_I that the suspension is dilute; a value of U_I of 0.65 m/s is sufficiently modest to be attainable in the near-shore environment by wave action or river inflow.

The ignition state of the three-equation model is not explored in more detail. The values are similar to those of the four-equation model, which will later be shown to be the superior of the two models.

The standard step method can be used to obtain numerical solutions to (17*a*–*c*). Upstream values U_0, ψ_0 and h_0 are specified, and the downstream development of the current is computed. All such currents are found to either ignite or subside. The solutions may be represented in terms of a phase space (U, ψ, h). Herein, for simplicity of presentation, this phase space is projected onto the phase plane (U, ψ), which is further normalized into the form $(U/U_I, \psi/\psi_I)$.

In figure 5, such a phase plane has been computed for the case of table 1 pertaining to the three-equation model; $h_0/D_s = 2 \times 10^4$, $c_D = 0.004$, $D_s = 0.1$ mm and $S = 0.05$. Only that part of the plane for which $Ri < 1$ is of interest herein. It is seen that this region is divided into igniting and subsiding subregions by the autosuspension generation line (AGL). A given current first tends to accelerate or decelerate toward the convergence line (CL). This 'backwater effect' occurs in open-channel flow, and has been described for conservative density currents by Ellison & Turner (1959). It is controlled by the difference between the upstream Richardson number and the Richardson number of the convergence line.

The convergence line is in fact a narrow band rather than a single line, the band resulting from a projection of a space onto a plane. Part of the convergence line is computed using the ignition values U_I and ψ_I as upstream values. In this case, and in fact in all cases involving the use of the three-equation model, a current eventually accelerates from ignition. The ignition point, however, is seen to be very close to the autosuspension generation line.

	D_s(mm)	c_D	S	h_0(m)	U_I(m)	ψ_I(m²/s)	C_I	Ri_I	K_I(m²/s²)
Three-equation model	0.1	0.004	0.05	2.0	0.652	3.78×10^{-3}	2.90×10^{-3}	0.221	—
		c_{D*}							
Four-equation model	0.1	0.004	0.025	2.0	1.162	2.65×10^{-2}	1.14×10^{-2}	0.272	2.13×10^{-2}
	0.1	0.004	0.05	0.5	0.967	1.13×10^{-2}	2.34×10^{-2}	0.203	2.40×10^{-2}
	0.1	0.004	0.05	2.0	0.874	8.29×10^{-3}	4.74×10^{-3}	0.201	1.83×10^{-2}
	0.1	0.004	0.05	8.0	0.798	6.26×10^{-3}	9.80×10^{-4}	0.199	1.41×10^{-2}
	0.1	0.004	0.1	2.0	0.736	3.57×10^{-3}	2.42×10^{-3}	0.144	1.64×10^{-2}
	0.1	0.002	0.05	2.0	1.193	2.01×10^{-2}	8.40×10^{-3}	0.191	2.02×10^{-2}
	0.1	0.01	0.05	2.0	0.613	3.18×10^{-3}	2.59×10^{-3}	0.223	1.66×10^{-2}
	0.2	0.004	0.05	2.0	1.834	7.44×10^{-3}	1.01×10^{-2}	0.195	6.21×10^{-2}
	0.04	0.01	0.05	0.08	0.194	1.13×10^{-4}	7.28×10^{-3}	0.250	2.51×10^{-3}
	0.04	0.01	0.05	0.16	0.185	9.62×10^{-5}	3.26×10^{-3}	0.247	2.19×10^{-3}
	0.04	0.01	0.05	0.32	0.179	8.73×10^{-5}	1.52×10^{-3}	0.245	2.01×10^{-3}
	0.04	0.02	0.05	0.16	0.138	4.97×10^{-5}	2.26×10^{-3}	0.308	2.06×10^{-3}
	0.04	0.004	0.05	0.16	0.283	2.92×10^{-4}	6.44×10^{-3}	0.208	2.46×10^{-3}
	0.04	0.004	0.05	0.80	0.252	2.05×10^{-4}	1.02×10^{-3}	0.207	1.88×10^{-3}

TABLE 1. Typical values at ignition.

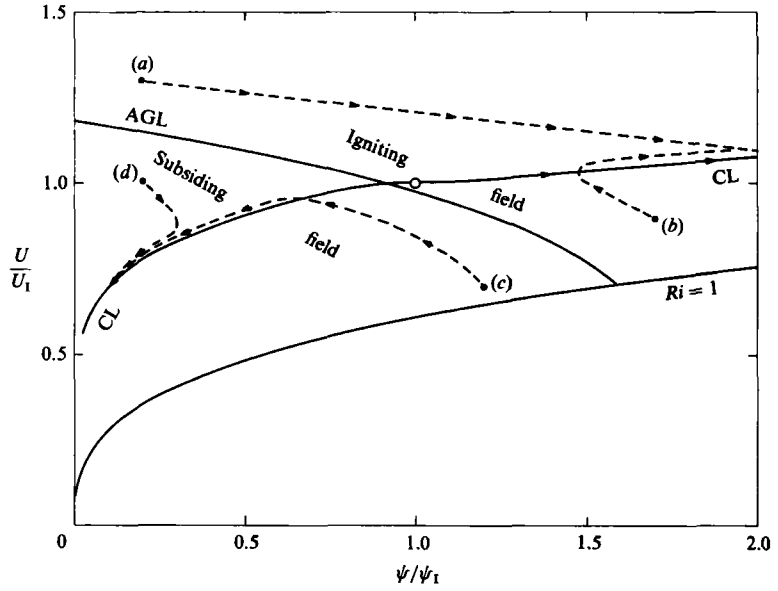

FIGURE 5. Phase diagram computed from the three-equation model, for the case $D_s = 0.1$ mm, $c_D = 0.004$, $S = 0.05$ and $h_0/D_s = 2\times10^4$. ○, ignition point; AGL, autosuspension generation line; CL, convergence line.

In figures 6 and 7 (*a–d*), the development of currents commencing from the ignition point, and from points (*a*), (*b*), (*c*) and (*d*) of figure 5, are shown. The currents so calculated are not necessarily physically possible. In particular, the three igniting currents show an extremely rapid increase in the sediment transport rate ψ. This increase is driven by values of the entrainment rate of bed sediment that far exceed the deposition rate, i.e.

$$\frac{\psi_e}{\psi} \gg 1$$

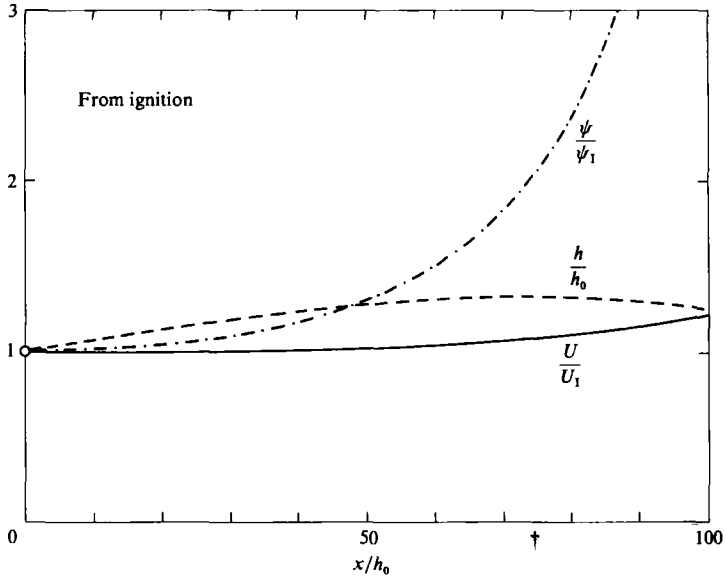

FIGURE 6. Current development from the ignition point of figure 5. The condition (16) fails to be satisfied downstream of the dagger.

in (17*b*), or using (18) $E_s \gg r_0 C$. In fact E_s is so large that the energy constraint (16) fails to be satisfied for all points downstream of the dagger in figures 6, 7(*a*, *b*). In general, it is found that none of the flows in the igniting subregion of figure 5 are physically possible; E_s is so large that the turbulent energy consumed in entraining new bed sediment would cause the turbulence to collapse.

This breakdown of the three-equation model is not peculiar to the particular values of D_s, S, c_D, and h_0 chosen for the above example, but rather occurs over a wide range of parameters. As a result, the model is not investigated in more detail.

7. Closure for the four-equation model

The failure to include an explicit accounting of the energy balance of the turbulence is the cause of the breakdown of the three-equation model. According to (21), (22) and (23), the sediment entrainment coefficient E_s is linked to u_*; by (25), it is further linked to flow velocity U. This linkage is crucial to the mass–momentum interaction between (17*b*) and (17*c*) that gives rise to ignition, but as ignition proceeds E_s becomes so large that constraint (16) fails.

The essential factor in entraining bed sediment is not, however, the magnitude of the velocity U, but rather the state of the turbulence, as can be seen from (2) and (A 19). In a more properly constituted model, then, E_s might be specified as an increasing function of the level of turbulence K. If the equation of energy balance of the turbulence (17*d*) were included explicitly in the model, large values of E_s would damp the turbulence, reducing K until smaller, sustainable values of K and E_s are realized. As a result, lower but sustainable rates of ignition might be possible.

Such linkage is established herein through the shear velocity u_*. In particular, the previous closure assumptions for r_0, e_w and E_s are retained, so that E_s is still a function of u_*. Closure assumption (25), however, is replaced with the assumption for fully turbulent flow

$$u_*^2 = \alpha K, \tag{26}$$

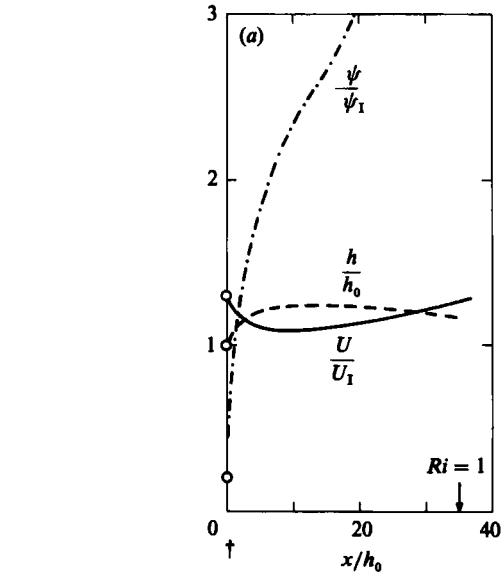

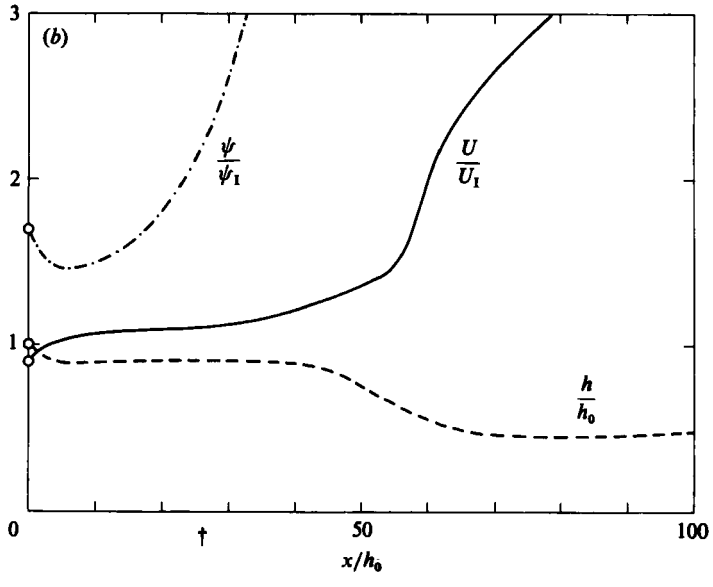

FIGURE 7(*a*,*b*). For caption see p. 158.

where α is approximated to be constant for a given flow. Using (A 13), (A 26) and (A 36*b*), and setting the velocity shape factor ζ_u equal to unity, (26) approximates to

$$-\overline{u'w'}|_{z=b} = \frac{1}{2}\frac{\alpha}{h}\int_0^\infty \overline{(u'^2+v'^2+w'^2)}\,\mathrm{d}z. \tag{27}$$

The linkage provided by (27) relates one turbulent quantity to another, and is thus in one sense more reasonable than that provided by (25). It can be criticized in that it relates one near-bed turbulent quantity with another layer-averaged quantity,

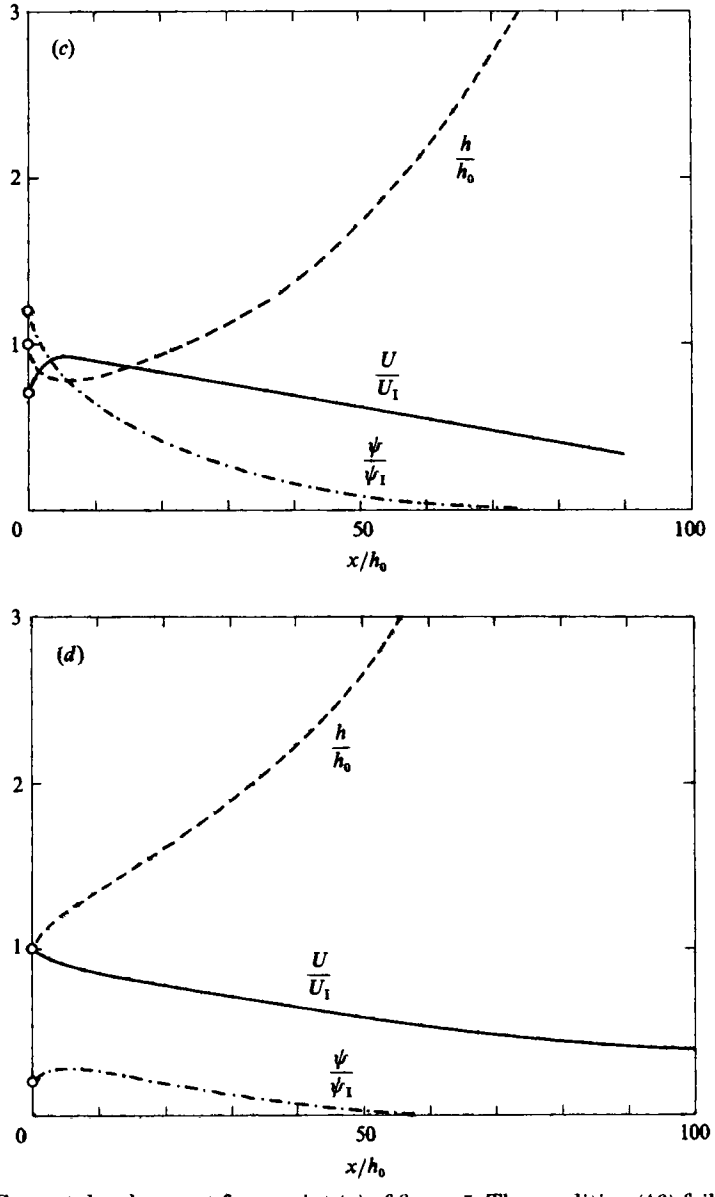

FIGURE 7. (*a*) Current development from point (*a*) of figure 5. The condition (16) fails to be satisfied downstream of the dagger, here at the origin. (*b*) Current development from point (*b*) of figure 5. The condition (16) fails to be satisfied downstream of the dagger. (*c*) Current development from point (*c*) of figure 5. (*d*) Current development from point (*d*) of figure 5.

that is, the near-bed Reynolds stress may not be closely linked to the turbulence produced in the shear layer above the peak in mean velocity (see figure 1), even though K includes a contribution from this region. A similar criticism, however, could be levelled at the three-equation model, and indeed at any layer-integrated treatment.

Equation (25) can be retained as a definition for c_D, which now becomes a computed rather than a specified parameter. Even if α is constrained to be constant

for a given flow, it is seen from (25) and (26) that c_D no longer need be constant in time or in space for that flow, as

$$c_D = \alpha \frac{K}{U^2}, \tag{28}$$

that is c_D is proportional to the ratio of turbulent kinetic energy to the kinetic energy of the mean flow.

The four-equation model thus consists of (17*a–d*) with the previous closure assumptions for r_0, E_s and e_w and (26) for u_*. One more closure hypothesis is required, however; in (17*d*), it is necessary to have an independent expression for the viscous dissipation rate ϵ_0. Since at least the time of Kolmogorov (see Launder & Spalding 1972) the following type of assumption has been widely used:

$$\epsilon_0 = \beta \frac{K^{\frac{3}{2}}}{h}. \tag{29}$$

The dimensionless parameter β is presumably related to other flow parameters. Herein a treatment of simple, conservative density currents is used to obtain an approximate expression for β.

As pointed out previously, with regard to the three-equation model, the case of the conservative density current is realized by setting $v_s = 0$ in (17*a–d*). The four-equation model also admits equilibrium solutions, but in this case K is constant, as are U, ψ and (by implication) Ri. Equation (17*a*) again reduces to

$$\frac{\mathrm{d}h}{\mathrm{d}x} = e_w(Ri),$$

so that layer thickness increases linearly downstream.

Herein β is evaluated for a simple, conservative density current by requiring that the three-equation and four-equation models predict the same equilibrium state. To this end, a particular current with specified values of U, C and h at some point is considered. Let c_{D*} be the coefficient of bed friction that this current would possess if it were indeed at equilibrium, i.e. the associated equilibrium coefficient of bed friction. According to the three-equation model, (25) dictates that

$$c_D = c_{D*},$$

whether or not the current is in fact at equilibrium. In the four-equation model, however, c_D is given by (28), and is equal to c_{D*} only at that particular value of K associated with equilibrium flow; i.e.

$$c_{D*} = \alpha \frac{K}{U^2}\bigg|_{\text{equilibrium}}. \tag{30}$$

If (29) and (30) are inserted into (17*d*) and reduced for the case of spatial equilibrium with v_s vanishing, it is found that

$$\beta = \frac{\frac{1}{2}e_w\left(1 - Ri - 2\frac{c_{D*}}{\alpha}\right) + c_{D*}}{\left(\frac{c_{D*}}{\alpha}\right)^{\frac{3}{2}}}. \tag{31}$$

It is easily verified that the use of (30) in (17*c*) ensures that the equilibrium relations between U, C and h obtained from the three-equation model are identical to those

obtained from the four-equation model for the case $v_s = 0$; thus both models predict the same normal Richardson number.

The local turbulent viscous dissipation rate ϵ, and thus its layer average ϵ_0, are non-negative quantities, vanishing only when there is no turbulence. It follows from (29) that β must be positive. In (31), c_{D*} and α are positive. Since in addition e_w is also non-negative it follows from (31) that β is positive if

$$Ri < \left(1 - 2\frac{c_{D*}}{\alpha}\right) + 2\frac{c_{D*}}{e_w}.$$

It is seen from (30) that the ratio $2c_{D*}/\alpha$ equals the ratio of mean turbulent energy to the energy of the mean flow. This ratio can be expected to be small for the type of flows under consideration herein. The term in brackets on the right-hand side of the above inequality will therefore be greater than Ri for most supercritical flows ($Ri < 1$), excepting only those with a Richardson number very close to unity. Near the condition $Ri = 1$, however, e_w drops drastically and for subcritical flows ($Ri > 1$), e_w becomes so small that it can be taken to vanish as an approximation. The final term on the right-hand side of the inequality thus becomes very large for subcritical and only slightly supercritical flow, so β can be expected to be positive in general.

It is now proposed that (31), obtained from considerations of equilibrium flow of simple density currents, be extended as an approximation to the case of disequilibrium turbidity currents, and used in the four-equation model. It should be noted that even in the case of a simple density current, the solutions for disequilibrium flow (and in particular, the disequilibrium value of c_D) from the four-equation model can be expected to differ from those obtained from the three-equation model. In the three-equation model, then, c_D is a specified parameter, whereas in the four-equation model, the parameter α and the associated equilibrium coefficient of bed friction c_{D*} are specified, and the actual value of c_D is then computed by solving for the flow.

8. Test of the four-equation model

The closure scheme of the four-equation model differs from the more familiar scheme of the three-equation model, and thus requires verification. Data pertaining specifically to turbidity currents are not available. In the case $Ri = v_s = 0$, however, the governing equations (17*a–d*) were used to study the limiting case of a plane wall jet.

Rajaratnam (1976) has summarized experimental data from five researchers on plane wall jets; the points in figure 8(*a*) have been adapted from figure 10-7 therein, with the addition of the data of Mathieu & Tailland (1965). The four-equation model was used to compute jet development downstream of a point twenty nozzle thicknesses downstream of the actual inlet, to avoid complications associated with the potential core. It was found that the data could be predicted with the three-equation model using a value of e_w of 0.05; accordingly, the same value was used in the four-equation model. The data corresponds to various bed-friction factors, but fortunately wall jet velocity U is only weakly dependent on bed friction. Accordingly, calculations were performed using values of the equilibrium coefficient of bed friction c_{D*} ranging from 0.002 to 0.01.

In figure 8(*a*), the curves represent velocity plotted as a function of downstream distance, with c_{D*} as an auxiliary parameter. Also α has been set equal to 0.1, and

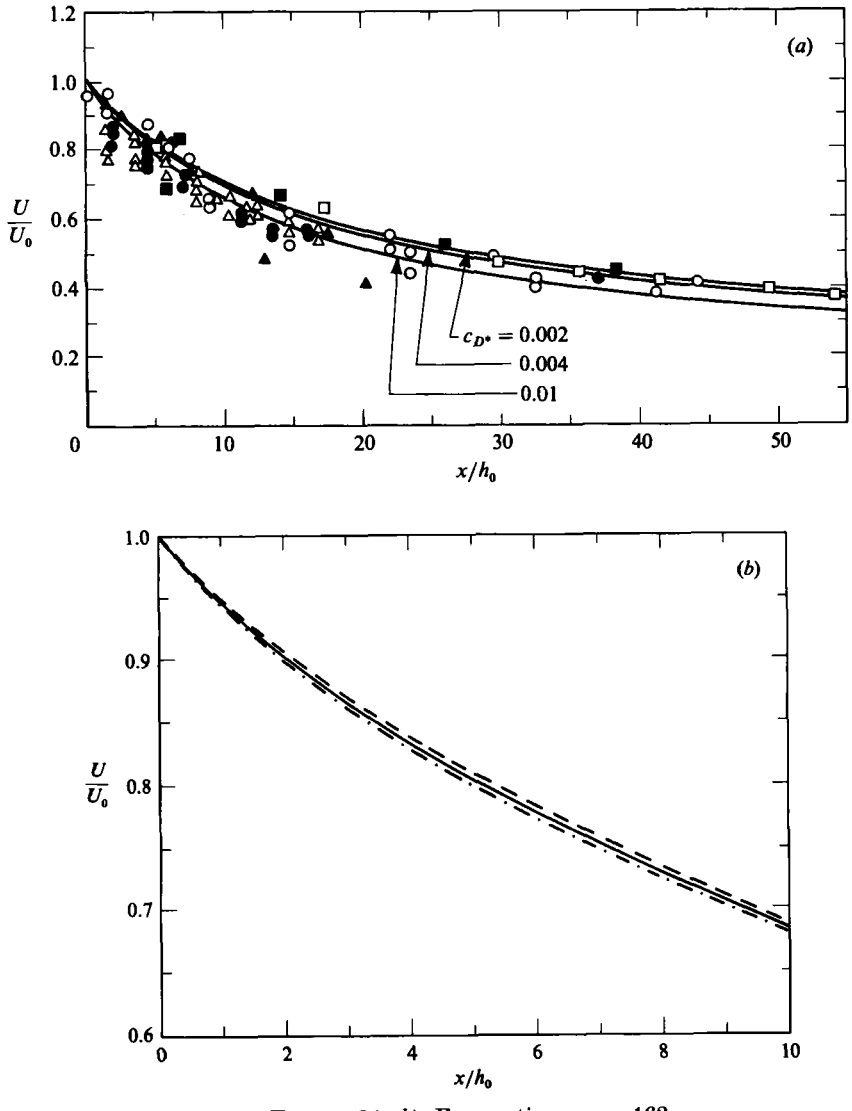

FIGURE 8(*a*,*b*). For caption see p. 162.

it is furthermore assumed that the actual upstream friction factor c_{D0}, seen from (28) to be given by

$$c_{D0} = \frac{\alpha K_0}{U_0^2},$$

is set equal to the equilibrium value c_{D*}. This assumption implies that the turbulence is completely developed. It is seen that the agreement is reasonable over the chosen range of values of c_{D*}.

In figure 8(*b*), the effect of varying the upstream level of turbulence is studied. That is, c_{D0} is allowed to vary from a vanishing value, corresponding to the absence of inlet turbulence, to a value corresponding to double the equilibrium level of turbulence. Again α is set equal to 0.1, and c_{D*} is 0.004. The effect of the initial level of turbulence on jet development is seen to be very small.

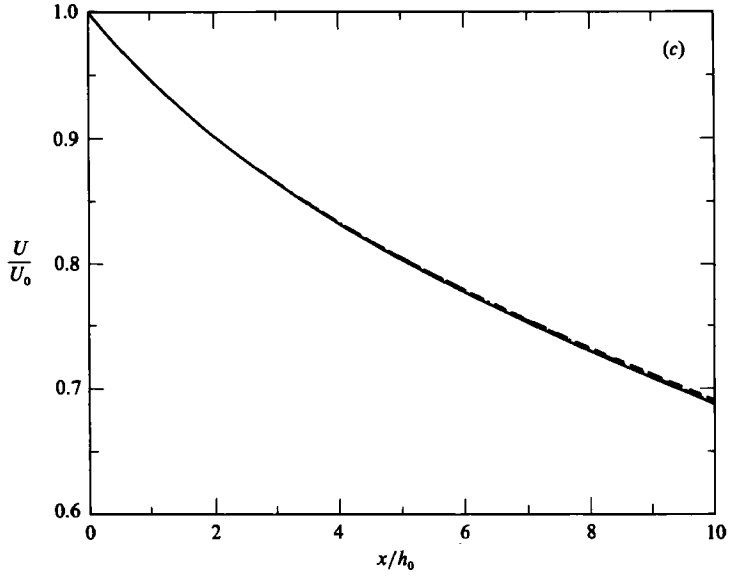

FIGURE 8. (*a*) Plot of U/U_0 *vs.* x/h_0 for plane wall jets, showing the effect of varying c_{D*} on the predictions of the four-equation model. The points represent experimental data. ○, Myers *et al.* (1961); ●, Sigalla (1958); △, Schwarz & Cosart (1961); ■, Gartshore & Newman (1969); ▲, Rajaratnam (1976); □, Mathieu & Tailland (1965). The curves represent calculations based on the four-equation model. $\alpha = 0.1$. (*b*) Plot of U/U_0 *vs.* x/h_0 for plane wall jets, showing the effect of varying c_{D0} on the predictions of the four-equation model. – – –, $c_{D0} = 0$; ——, 0.004; –·–·–, 0.008. $c_{D*} = 0.004$, $\alpha = 0.1$. (*c*) Plot of U/U_0 *vs.* x/h_0 for plane wall jets, showing the effect of varying α on the predictions of the four-equation model. ——, $\alpha = 0.05$; –·–·–, 0.1; – – –, 0.5. $c_{D*} = 0.004$, $c_{D0} = 0.004$.

Likewise, in figure 8(*c*) the effect of varying α is studied, for the case $c_{D0} = c_{D*} = 0.004$. The downstream development of jet velocity is seen to be essentially independent of α as it varies from 0.05 to 0.5.

In conclusion, the four-equation model can be used to predict the development of flow velocity U in plane wall jets.

9. Computations with the four-equation model

Analogously to the three-equation model, an ignitive state for the four-equation model can be defined in terms of the lowest roots U_I, ψ_I and K_I such that the right-hand sides of (17*b–d*) vanish for a given value of h_0. Again the ignitive state is not a true equilibrium, but proves useful in quantifying ignition versus subsidence of a current.

For the case of the four-equation model S, c_{D*}, h_0/D_s, R_p (or rather D_s herein) and α must be specified in order to determine the ignition values U_I, ψ_I, and K_I. Very little information is available concerning the value of α. The data of Mathieu & Tailland (1965) for wall jets suggest a value of about 0.1, but different values might be expected for a density-driven flow. Fortunately, the dependence of U_I and ψ_I, (and thus C_I) on α is exceedingly weak. In particular, in the limit as v_s vanishes, the ignition state is replaced by a true equilibrium; the equilibrium values of U, ψ and C can be shown to be strictly independent of the value of α. As long as v_s/U remains small, as can be expected to be the case for most turbidity currents of interest, not only the ignition values U_I, ψ_I and C_I, but also the downstream development of U,

α	U_I(m/s)	C_I	K_I(m²/s²)	u_{*I}(m/s)	β
0.05	1.24	5.04×10^{-3}	7.98×10^{-2}	6.32×10^{-2}	0.305
0.10	1.24	5.04×10^{-3}	3.99×10^{-2}	6.32×10^{-2}	0.905
0.50	1.23	4.97×10^{-3}	7.97×10^{-3}	6.31×10^{-2}	10.5

TABLE 2. Values of parameters at ignition for various values of α; $D_s = 0.15$ mm, $c_{D*} = 0.004$, $S = 0.08$, and $h_0 = 3$ m. Calculations are based on the four-equation model

α	U(m/s)	C	h(m)
0.05	1.93	5.21×10^{-3}	8.10
0.10	1.98	5.68×10^{-3}	7.91
0.50	1.94	5.39×10^{-3}	7.99

TABLE 3. Values of U, C and h computed 1000 m downstream from the origin, using the parameters of table 2. The computations commence from ignition.

ψ, C and h, can be shown to be only weakly dependent on the value of α. Some examples are presented in tables 2 and 3 for the case $D_s = 0.15$ mm, $c_{D*} = 0.004$, $S = 0.08$, and $h_0 = 3$ m, chosen to be typical of Scripps Submarine Canyon (Inman *et al.* 1976; Fukushima *et al.* 1985). As α varies over an order of magnitude from 0.05 to 0.5, U_I varies by less than 1 %, and C_I varies by less than $1\frac{1}{2}$%. The reason for this is apparent from the values of u_*. K_I itself varies over an order of magnitude in α; the values of u_* computed from (26), however, are seen to be essentially constant. Since u_* characterizes the bed resistance and controls the sediment entrainment rate E_s, the near-constancy of U_I and C_I follows. Based on these considerations, α is set equal to 0.1 herein.

Values of U_I, C_I, ψ_I, Ri_I and K_I computed from the four-equation model for a variety of D_s, S, c_{D*} and h_0 are shown in table 1. Comparing the results for the case $D_s = 0.1$ mm, $S = 0.05$, $c_{D*}(c_D) = 0.004$ and $h_0 = 2$ m, it is seen that the values of U_I, C_I and Ri yielded by the three-equation and four-equation models are rather similar. Henceforth all results concerning ignition pertain to the four-equation model.

In figure 9(*a*, *b*, *c*) U_I, C_I and Ri_I respectively, are plotted as functions of h_0/D_s, and the auxiliary parameters S and D_s; c_{D*} is set equal to 0.004. It is seen that higher slopes and finer sediment (as long as it is non-cohesive) are conducive to reducing the values of U_I and C_I. In figure 9(*c*) it is seen that the ignition Richardson number Ri_I is almost independent of h_0 and D_s, but strongly dependent on S, for a given value of c_{D*}.

In figure 10(*a*, *b*) Ri_I and C_I respectively, are plotted as functions of S, with c_{D*} and D_s as auxiliary parameters; h_0/D_s is set equal to 2×10^4. It is seen that Ri_I is not strongly dependent on c_{D*}. Figure 10(*b*) suggests the difficulty of attaining the ignition state with coarse sediment on low slopes.

The standard step method is again used, this time to solve (17*a–d*) numerically, for the downstream development of currents with prescribed upstream values U_0, ψ_0, h_0 and K_0. In order to reduce the number of cases to be computed, and allow for projection of the results onto a $(U/U_I, \psi/\psi_I)$ phase plane, K_0 was not allowed to vary freely. The following simple rule was applied in selecting K_0:

$$\frac{K_0}{U_0^2} = \frac{K_I}{U_I^2}. \tag{32}$$

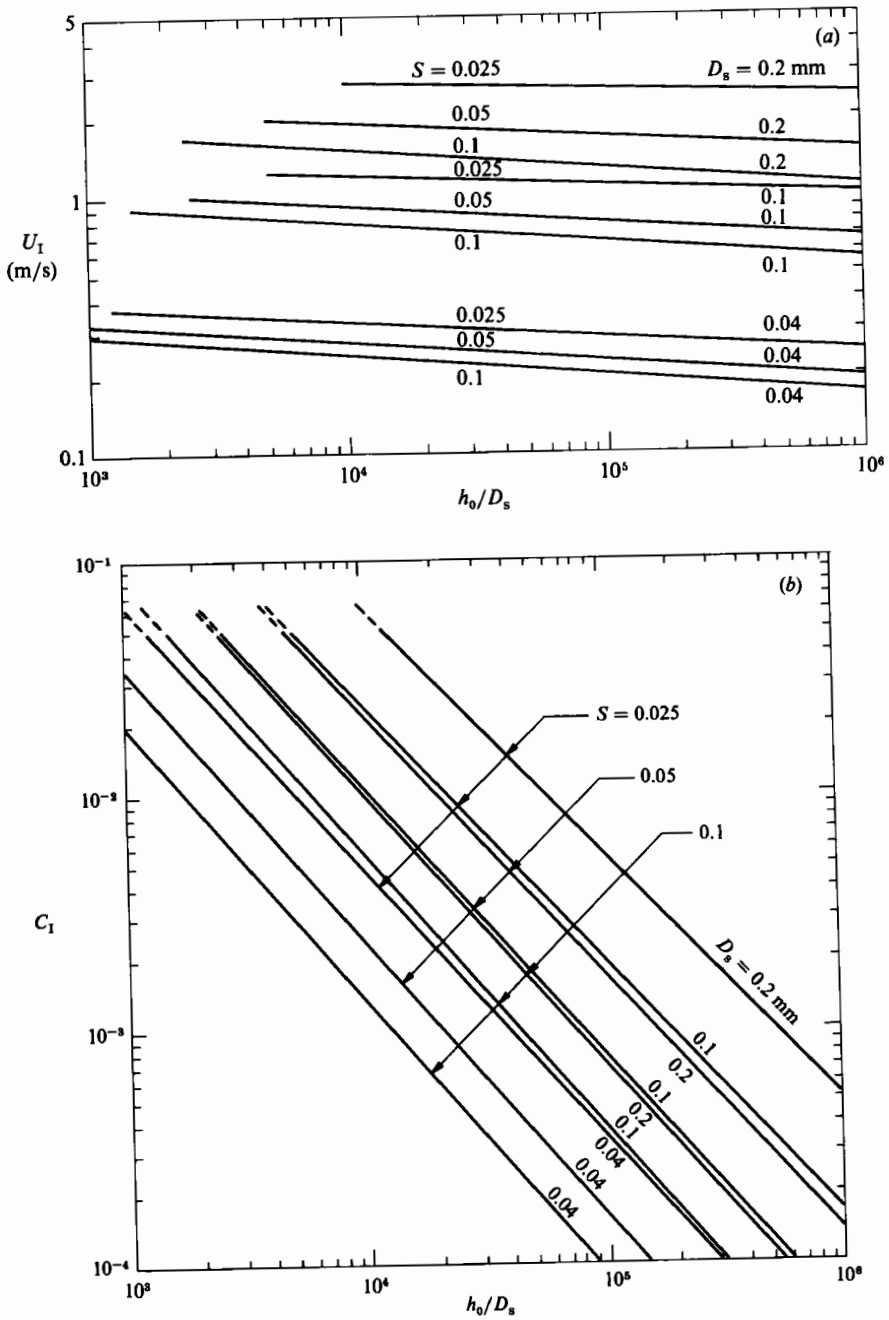

FIGURE 9(*a*,*b*). For caption see facing page.

Physically, (32) can be interpreted as follows. The ratio of turbulent energy to mean flow energy at $x = 0$ is always set equal to the value at ignition. From (28), it is seen that (32) equivalently implies that the initial bed-resistance coefficient c_D is always equated to the value at ignition (which can be expected to differ somewhat from the value associated with an equilibrium conservative density current, c_{D*}). It should be emphasized, however, that the use of (32) is purely a matter of convenience.

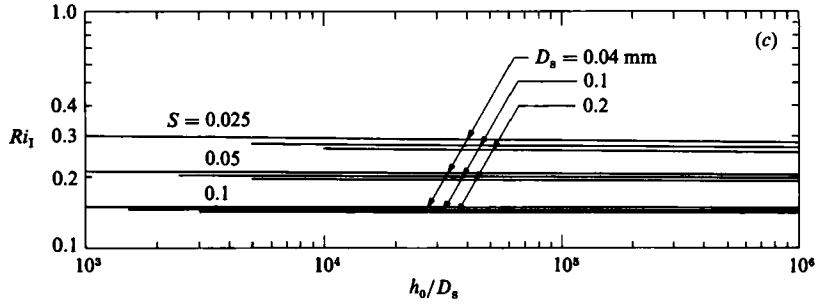

FIGURE 9. (*a*) Plot of U_I *vs.* h_0/D_s for the four-equation model; (*b*) C_I *vs.* h_0/D_s for the four-equation model; (*c*) Ri_I *vs.* h_0/D_s for the four-equation model. $c_{D*} = 0.004$; D_s and S serve as auxiliary parameters.

A current with upstream values U_0, ψ_0 and h_0 that subsides if K_0 is computed from (32), may indeed ignite if K_0 is taken to be substantially higher. In particular, the value of K_0 computed from (32) might be reasonable where the turbidity current is a natural continuation of deltaic river flow, but might be too conservative where the turbidity current is generated by edge wave action, as is the case for Scripps Submarine Canyon (Inman *et al.* 1976).

In figure 11, a phase-plane projection analogous to that of figure 5 has been constructed using the four-equation model. Again $D_s = 0.1$ mm, $c_{D*} = 0.004$, $S = 0.05$, and $h_0/D_s = 2 \times 10^4$. A comparison of figures 5 and 11 indicates qualitative agreement between the predictions of the three-equation and four-equation models. Although the absolute values of U_I and ψ_I are larger in the case of the four-equation model, the autosuspension generation line is displaced downward in figure 11 compared with figure 5. As a result, the predictions of the two models as regards whether a given current ignites or subsides do not differ greatly.

Both the ignition and subsidence of currents predicted by the four-equation model are, however, subdued compared with the three-equation model. The downstream development of U, ψ and h computed from ignition are shown in figure 12, and the cases of currents igniting from points (*a*) and (*b*) of figure 11 are shown in figure 13(*a*, *b*). A comparison of figures 12 and 6, 13(*a*) and 7(*a*), and 13(*b*) and 7(*b*) indicates that the increase in ψ in the downstream direction, while marked, is far less rapid in the case of the four-equation model. In fact, the structure of the four-equation model is such that rapid ignition leading to the collapse of the turbulence cannot occur. If E_s is too large, according to (8) and (17*d*), K is reduced; this reduces u_* according to (26), and thus consequently E_s. As a result ψ increases less rapidly, and the acceleration is sustainable in terms of the balance of turbulent energy.

The downstream increase in velocity in the case of figures 12 and 13(*a*, *b*) is rather modest, even at a point 1000 m downstream of the canyon head. Although not shown on the figures, substantially higher velocities are reached farther downstream. In the case of the curve shown in figure 12, a velocity equal to 2.3 times the upstream value is obtained 3000 m downstream of the canyon head.

In figure 13(*c*, *d*) subsidence predicted by the four-equation model from points (*c*) and (*d*) of figure 11 is shown. The subsidence is much less rapid than that predicted by the three-equation model.

In figure 14 the ratio of turbulent kinetic energy to the energy of the mean flow, $K/(\frac{1}{2}U^2)$, is plotted for the five cases corresponding to figures 12 and 13(*a–d*). There is a substantial damping of turbulence, and thus a reduction of the bed-resistance coefficient c_D according to (28), for the three igniting currents. The opposite

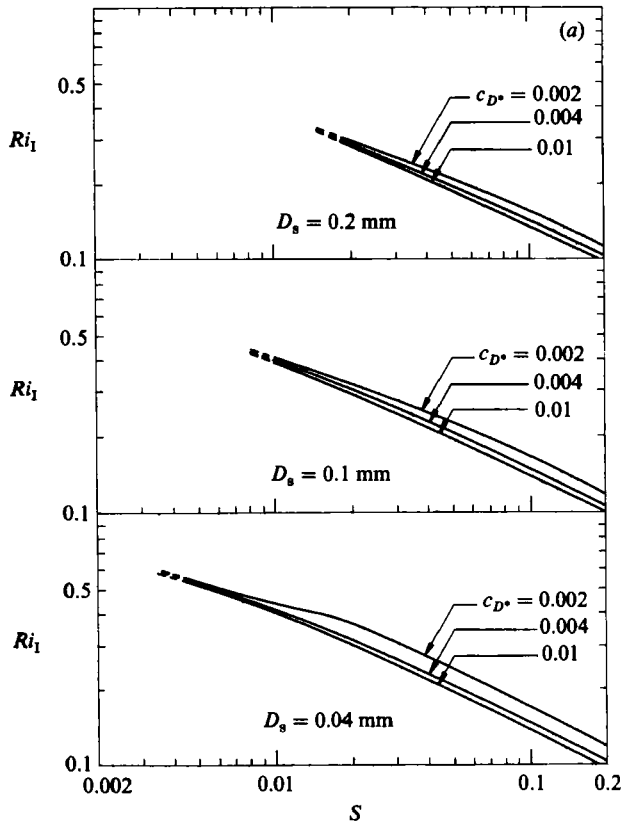

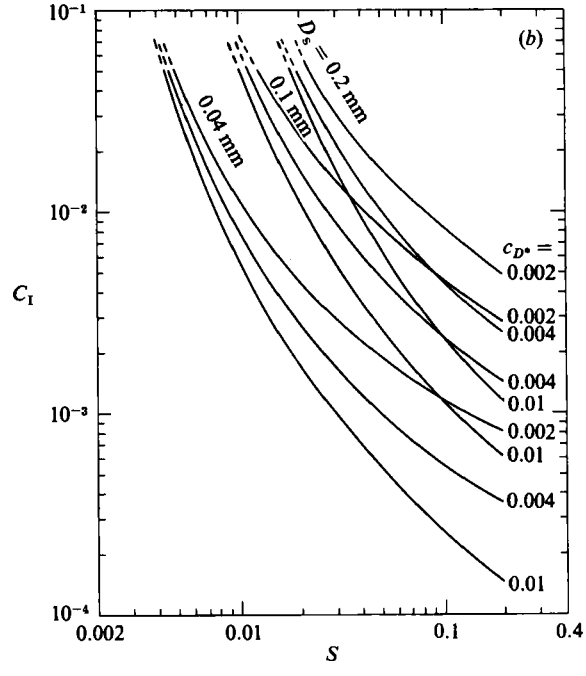

FIGURE 10. (*a*) Plot of Ri_1 *vs.* S and (*b*) C_1 *vs.* S, for the case $h_0/D_s = 2 \times 10^4$; D_s and c_{D^*} serve as auxiliary parameters.

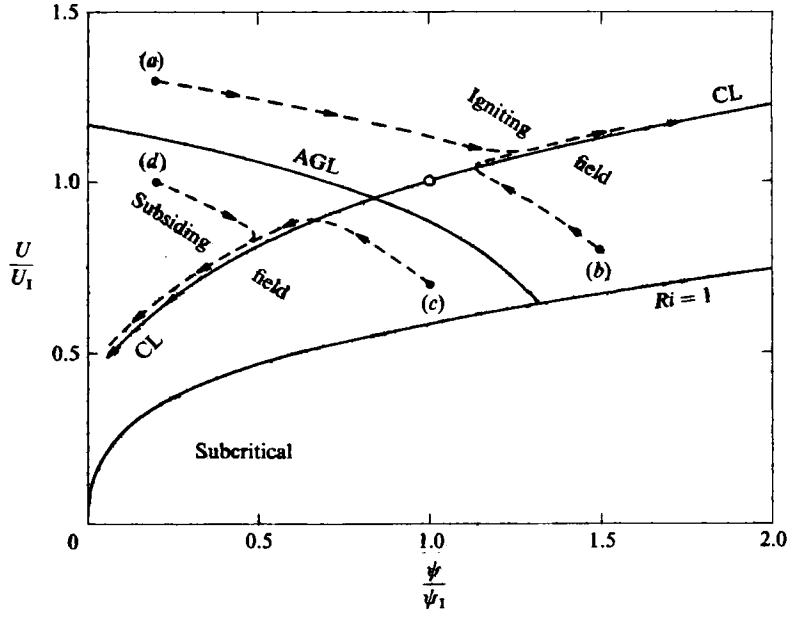

FIGURE 11. Phase diagram computed from the four-equation model, for the case $D_s = 0.1$ mm, $c_{D*} = 0.004$, $S = 0.05$, and $h_0/D_s = 2 \times 10^4$: ○, ignition point.

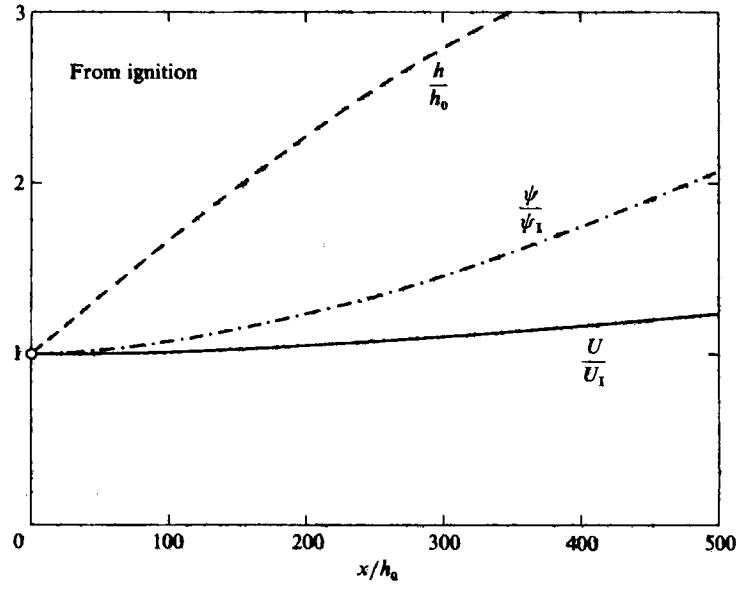

FIGURE 12. Current development from the ignition point of figure 11.

behaviour is shown for the two subsiding currents. In the three-equation model, on the other hand, the bed-resistance coefficient is specified beforehand (constant values have been assumed herein).

The drop in the coefficient of bed resistance is not associated with any particular ease of acceleration. The acceleration realized in the case of the three-equation model is much more rapid, even though c_D is held constant.

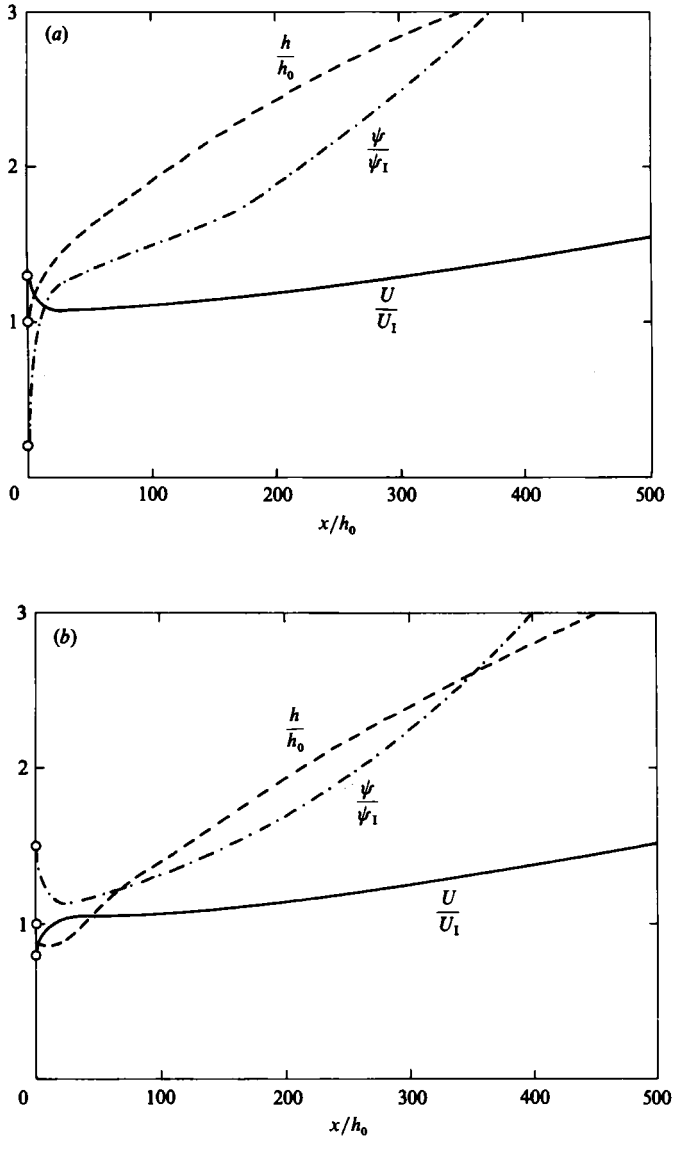

FIGURE 13(*a*, *b*). For caption see facing page.

One aspect of the four-equation model is the existence of damped periodic ('wavy') solutions. This type of behaviour can be seen in the initial parts of some of the curves presented here, notably in figure 13(*a–c*).

Figure 15 shows the downstream development of the Richardson number, based on the results of calculations from ignition, with the conditions specified in figures 5 and 11. A characteristic of the four-equation model is the near-constancy of the Richardson number along the convergence line. On the other hand, along the igniting part of the convergence line of the three-equation model the Richardson number rapidly approaches unity, implying an incipient hydraulic jump. The near-constancy of the Richardson number along the convergence line of the four-equation model does not imply an equilibrium state, but rather that ψ increases (or decreases) as U^3, since

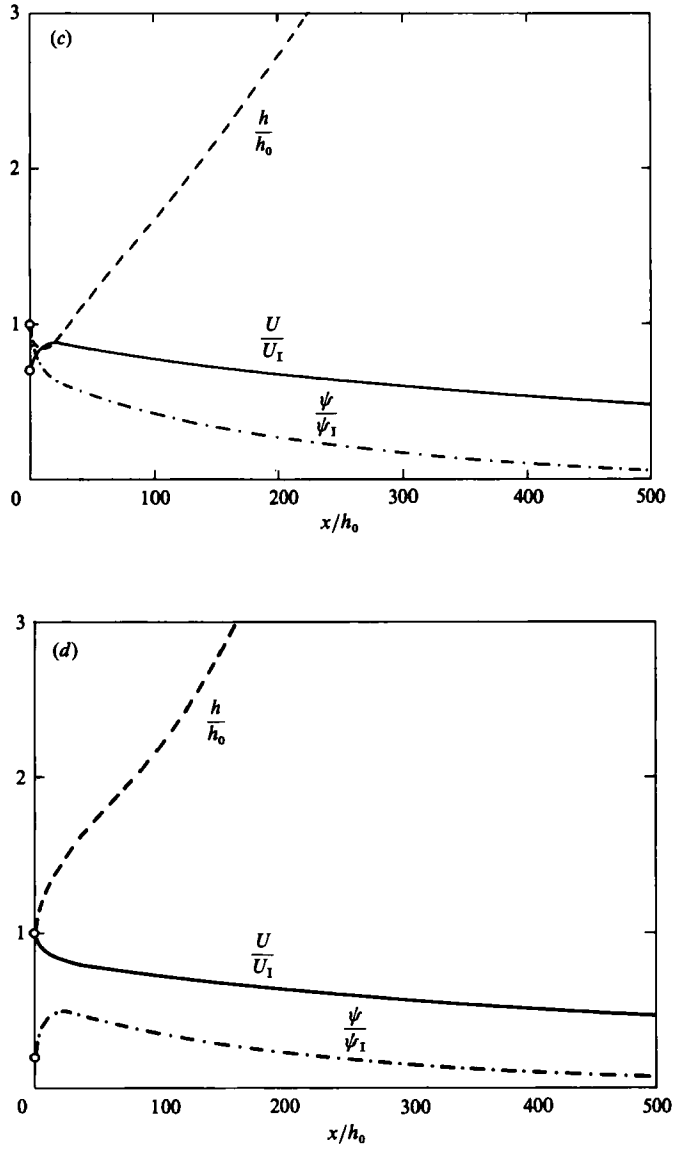

FIGURE 13. Current development (*a*) from point (*a*) of figure 11; (*b*) from point (*b*) of figure 11; (*c*) from point (*c*) of figure 11; (*d*) from point (*d*) of figure 11.

$$Ri = \frac{Rg\psi}{U^3}.$$

In figure 16(*a–d*), some indication of the sensitivity of the autosuspension generation line to variations in h_0/D_s, D_s (as a surrogate for R_p), c_{D^*} and S is provided. All diagrams are based on calculations using the four-equation model, and are plotted in the form of U/U_I *vs.* ψ/ψ_I so that the ignition point remains at (1, 1). Figure 16(*a*, *b*) show that the position of the autosuspension generation line is not very sensitive to variation in h_0/D_s and D_s. A somewhat more substantial variation in

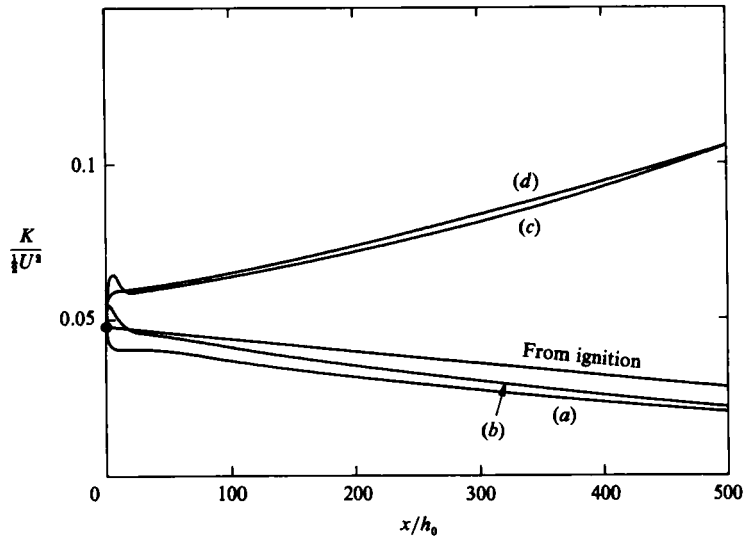

FIGURE 14. Ratio of mean turbulent kinetic energy to kinetic energy of the mean flow as a function of distance downstream for the cases of figures 12 and 13(*a–d*).

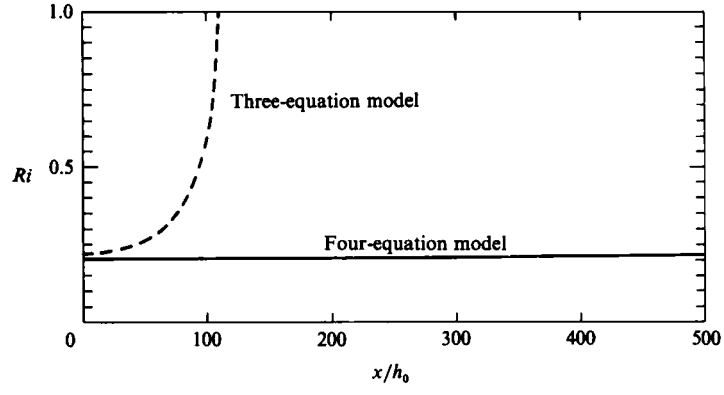

FIGURE 15. Comparison of the downstream development of the Richardson number in the cases of figure 6 (three-equation model computed from ignition) and figure 12 (four-equation model computed from ignition).

the autosuspension generation line is apparent in figure 16(*c*) as c_{D*} is varied; as c_{D*} increases, the region of ignition retreats upward. In addition, variation in c_{D*} is seen to cause a modest change in the position of the line corresponding to a Richardson number of unity. By far the largest variation is seen in figure 16(*d*) as S is varied, with a substantial upward retreat of the region of ignition as slope decreases. The implication is that ignition may be very difficult to achieve on low slopes.

Several calculations were performed to test the sensitivity of a developing current to variations in α. To this end, calculations were commenced from ignition, using the values shown in table 2. In table 3 values of U, C and h at a point 1000 m downstream of the mouth of the canyon are shown. The dependence on α is seen to be very weak.

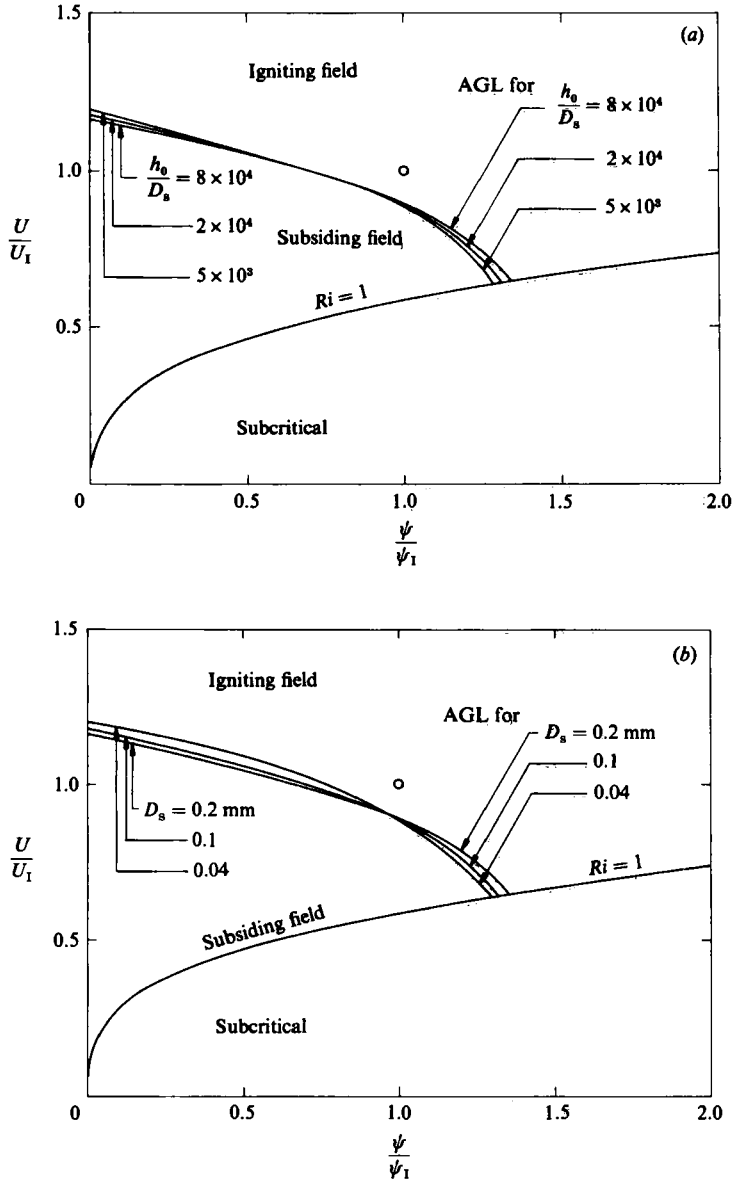

FIGURE 16(*a*,*b*). For caption see p. 172.

10. Conclusions

As indicated in the Introduction, the purpose of the present paper is a general exposition of the equations of motion of turbidity currents, their closure, and their solution for the continuous, spatially developing case in submarine canyons. Special emphasis is placed on the possibility of self-acceleration, or ignition, by means of the incorporation of bed sediment into the current.

The key approximations in the derivation of the layer-averaged equations are: the assumption of concentrations sufficiently small to allow for the use of the Boussinesq approximation, the boundary-layer approximations, the similarity assumptions, and

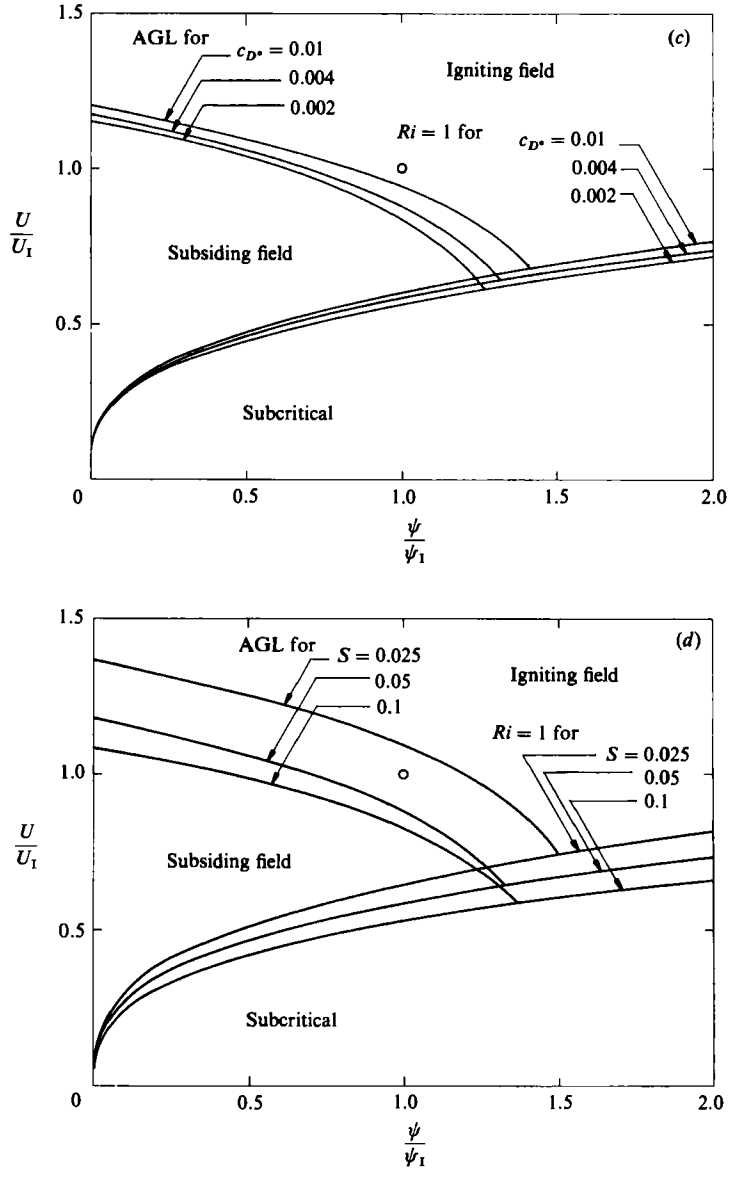

FIGURE 16. Sensitivity of a phase diagram to variation (*a*) in h_0/D_s ($c_{D^*} = 0.004$, $D_s = 0.1$ mm, $S = 0.05$); (*b*) in D_s ($c_{D^*} = 0.004$, $S = 0.05$, $h_0/D_s = 2 \times 10^4$); (*c*) in c_{D^*} ($D_s = 0.1$ mm, $h_0/D_s = 2 \times 10^4$, $S = 0.05$); (*d*) in S ($c_{D^*} = 0.004$, $D_s = 0.1$ mm, $h_0/D_s = 2 \times 10^4$). ○, ignition point.

the slab approximations for evaluating the shape coefficient. Some indication of the error involved in the last of these approximations is provided by Henderson-Sellers (1981) for the case of a plume.

Two models are presented. The first of these is the three-equation model, which can be considered to be a generalization of the model of Ellison & Turner (1959) for simple, conservative density currents to the case of eroding and depositing turbidity currents. It consists of relations for fluid mass conservation, sediment mass

conservation, and flow momentum conservation. The model is closed with appropriate assumptions for bed resistance, sediment entrainment from the bed, near-bed sediment concentration, and water entrainment from above. In particular, the bed shear stress is related to the mean velocity of the flow. Numerical solution reveals that if the upstream values of velocity U and sediment transport rate ψ are sufficiently large, strong ignition occurs, so that U and ψ increase markedly downstream. Ignition is caused by an interaction between the equations of flow momentum and sediment mass balance.

A consideration of the balance of mean turbulent energy reveals four important mechanisms contributing to the loss of turbulent energy. The first consists of viscous dissipation due to the turbulence. The remaining three all fall under the category of work done against the buoyancy gradient. They are the work needed to hold the existing concentration of sediment in suspension, the work expended in lifting the centre of gravity of the suspension as it is diluted by water entrained from above, and the work expended in lifting sediment entrained from the bed into the suspension. The last term represents an expenditure of energy only if the rate of entrainment of bed sediment exceeds the rate of deposition of sediment on the bed; in the opposite case, the term represents an energy gain.

A consideration of these terms leads to the delineation of a generalized Knapp–Bagnold-type energy constraint on turbid underflows. According to this constraint, if the net rate of supply of energy to the turbulence is less than the sum of the three terms representing the rate of working against the buoyancy gradient for a sufficient distance or amount of time, the turbulence must vanish, and the turbidity current must cease.

The constraint poses a problem for the three-equation model, which does not directly account for turbulent energy balance. The accelerative mechanism for igniting currents predicted by this model is so strong that extremely high rates of sediment entrainment result. The rates are often so high that the rate of turbulent energy expenditure due to the entrainment of bed sediment alone far exceeds the rate of production of turbulent energy. It follows that the solutions obtained for ignitive turbidity currents via the three-equation model are typically physically impossible.

Herein, this fault is remedied by the formulation of a four-equation model, in which a relation describing the balance of the mean energy of the turbulence is explicitly included. The bed shear stress, and thus the sediment entrainment coefficient E_s, is linked to the level of turbulent energy K rather than the flow velocity. In this fashion, if E_s is too high the associated loss of turbulent energy will act to reduce K, and thus reduce E_s to a more appropriate value. The closure assumptions for sediment entrainment from the bed, near-bed sediment concentration, and water entrainment from above are otherwise identical with those of the three-equation model. In addition, an appropriate closure assumption for viscous dissipation is introduced.

The predictions of the four-equation model appear reasonable, and presumably have applications to the genesis of submarine canyons. Very little data, however, are available with which to test the theory. Nearly all of those data pertain to Scripps Submarine Canyon; a detailed application of the four-equation model to this case has been carried out by Fukushima *et al.* (1985).

It is noted in closing that many aspects of the present model remain tentative in the absence of detailed observations taken under controlled conditions. Such observations would appear to be very difficult. In the light of this, the many specific predictions presented herein are intended to illustrate the general implications of the

present model rather than to suggest that all problems have been resolved. This tentative approach can perhaps be justified in the light of the difficulty of field observation.

Funding from the National Science Foundation (Grant No. NSF/EAR-8213045) and Sea Grant (Grant No. DOC/NA82AA-D-0039) is gratefully acknowledged.

This paper is published with the approval of the Director, British Geological Survey (NERC).

Appendix. Derivation of the layer-averaged equations

A.1. *Governing equations for a dilute suspension*

The geometry of figure 1 is considered. The quiescent body of water is assumed to be infinitely deep, and unstratified except for the turbidity current itself. The canyon cross-section is taken to be rectangular, with a width many times in excess of the thickness of the turbidity current. Variation in the lateral direction is neglected. The bed possesses a constant, small down-canyon slope S; the $x_1(x)$-coordinate is directed down-canyon tangential to the bed, and the $x_3(z)$-coordinate is directed upward normal to the bed.

The equations of motion for a suspension are considered. The suspension is assumed to be sufficiently dilute to justify the use of the Boussinesq approximation, and the assumption of a kinematic viscosity ν equal to the value for clear water. The equation of momentum conservation is

$$\frac{\partial \tilde{u}_i}{\partial t}+\frac{\partial \tilde{u}_i \tilde{u}_j}{\partial x_j}=-\frac{1}{\rho}\frac{\partial \tilde{p}_*}{\partial x_i}+\nu\frac{\partial^2 \tilde{u}_i}{\partial x_j \partial x_j}+(1+R\tilde{c})g_i, \tag{A 1}$$

where $\tilde{c}(x_i, t)$ denotes the instantaneous volumetric concentration of suspended sediment, $\tilde{u}_i(x_j, t)$ denotes the instantaneous flow velocity of the mixture, and $\tilde{p}_*(x_i, t)$ denotes the instantaneous pressure. The vector g_i is given by

$$g_i = g(S, 0, -1), \tag{A 2}$$

where g denotes the gravitational acceleration. Also ρ denotes the density of the quiescent fluid, and $R = (\rho_s/\rho - 1)$, where ρ_s is the material density of the sediment.

The equation of fluid mass conservation is

$$\frac{\partial \tilde{u}_i}{\partial x_i} = 0. \tag{A 3}$$

The velocity of the sediment phase is taken to be equal to the sum of the fluid velocity and the sediment fall velocity v_s in quiescent water; the equation of conservation of sediment thus becomes

$$\frac{\partial \tilde{c}}{\partial t}+\frac{\partial}{\partial x_i}[(u_i - v_s \delta_{i3})\tilde{c}] = 0, \tag{A 4}$$

where δ_{ij} denotes the Kronecker delta.

The hydrostatic pressure balance associated with the quiescent fluid can be subtracted from (A 1) by letting

$$\tilde{p}_* = p_s + \tilde{p},$$

where

$$\frac{\partial p_s}{\partial x_i} = \rho g_i.$$

Thus (A 1) reduces to

$$\frac{\partial \tilde{u}_i}{\partial t}+\frac{\partial \tilde{u}_i \tilde{u}_j}{\partial x_j}=-\frac{1}{\rho}\frac{\partial \tilde{p}}{\partial x_i}+\nu\frac{\partial^2 \tilde{u}_i}{\partial x_j \partial x_j}+R\tilde{c}g_i. \tag{A 5}$$

The parameters $\tilde{u}_i$, $\tilde{p}$ and $\tilde{c}$ are split into mean and fluctuating parts,

$$\tilde{u}_i = u_i+u_i'; \quad \tilde{p}=p+p'; \quad \tilde{c}=c+c'$$

in order to quantify the effect of turbulence. Standard techniques applied to (A 3), (A 4) and (A 5) yield the following relations averaged over turbulence: mean fluid mass conservation

$$\frac{\partial u_i}{\partial x_i}=0; \tag{A 6}$$

mean sediment conservation

$$\frac{\partial c}{\partial t}+\frac{\partial u_i c}{\partial x_i}=-\frac{\partial}{\partial x_i}(F_i-v_s c\,\delta_{i3}), \tag{A 7}$$

where

$$F_i=\overline{u_i' c'} \tag{A 8}$$

denotes the Reynolds flux of sediment; mean momentum conservation

$$\frac{\partial u_i}{\partial t}+\frac{\partial u_i u_j}{\partial x_j}=-\frac{1}{\rho}\frac{\partial p}{\partial x_i}+\frac{\partial}{\partial x_j}\left(\tau_{ij}+\nu\frac{\partial u_i}{\partial x_j}\right)+Rcg_i, \tag{A 9}$$

where

$$\tau_{ij}=-\overline{u_i' u_j'} \tag{A 10}$$

denotes the kinematic Reynolds stress; energy conservation of the mean flow

$$\frac{\partial}{\partial t}(\tfrac{1}{2}u_i u_i)+\frac{\partial}{\partial x_j}(u_j\tfrac{1}{2}u_i u_i)=-\frac{1}{\rho}u_i\frac{\partial p}{\partial x_i}+\frac{\partial}{\partial x_j}\left[u_i\tau_{ij}+\nu\frac{\partial}{\partial x_j}(\tfrac{1}{2}u_i u_i)\right]$$
$$+Rg_i u_i c-\tau_{ij}\frac{\partial u_i}{\partial x_j}-\nu\frac{\partial u_i}{\partial x_j}\frac{\partial u_i}{\partial x_j}; \tag{A 11}$$

and conservation of mean turbulent energy

$$\frac{\partial k}{\partial t}+\frac{\partial u_i k}{\partial x_i}=\tau_{ij}\frac{\partial u_i}{\partial x_j}+\nu\frac{\partial^2 k}{\partial x_j \partial x_j}-\frac{\partial}{\partial x_j}\left[\overline{u_j'\left(\frac{p'}{\rho}+\tfrac{1}{2}u_i' u_i'\right)}\right]-\nu\overline{\frac{\partial u_i'}{\partial x_j}\frac{\partial u_i'}{\partial x_j}}+RF_i g_i, \tag{A 12}$$

where

$$k=\tfrac{1}{2}\overline{u_i' u_i'}. \tag{A 13}$$

A.2. *Boundary-layer approximations for two-dimensional flow*

The slender-flow, or boundary-layer, approximations for a two-dimensional turbidity current are considered. Henceforth $x_i=(x,y,z)$ and $\tilde{u}_i=(\tilde{u},\tilde{v},\tilde{w})$. Variation in the lateral (y) direction is neglected. It is assumed that within the turbidity current, the scalings $u \gg w$ and $\partial/\partial z \gg \partial/\partial x$ hold. The turbidity current is assumed to be fully turbulent, with all viscous terms negligible except the viscous dissipation due to the turbulence. It is furthermore assumed that $|\overline{c'w'}| \gg |\overline{c'u'}|S$.

Under these constraints, the equation of mean fluid mass balance (A 6), becomes

$$\frac{\partial u}{\partial x}+\frac{\partial w}{\partial z}=0. \tag{A 14}$$

The upward component of mean momentum balance (A 9) reduces to

$$p=\rho Rg\int_z^\infty c\,\mathrm{d}z, \tag{A 15}$$

corresponding to the extra component of hydrostatic pressure due to the weight of the sediment. The down-canyon component of mean momentum balance (A 9) thus approximates to

$$\frac{\partial u}{\partial t}+\frac{\partial u^2}{\partial x}+\frac{\partial uw}{\partial z}=-Rg\frac{\partial}{\partial x}\int_z^\infty c\,\mathrm{d}z+RgcS+\frac{\partial \tau}{\partial z}, \tag{A 16}$$

where

$$\tau=\tau_{13}=-\overline{u'w'}. \tag{A 17}$$

The equation of mean sediment mass balance, (A 7), approximates to

$$\frac{\partial c}{\partial t}+\frac{\partial uc}{\partial x}+\frac{\partial wc}{\partial z}=-\frac{\partial}{\partial z}(F-v_s c), \tag{A 18}$$

where

$$F=F_3=\overline{c'w'}. \tag{A 19}$$

The equation of energy balance of the mean flow, (A 11), approximates with the aid of (A 15) to

$$\frac{\partial}{\partial t}(\tfrac{1}{2}u^2)+\frac{\partial}{\partial x}(\tfrac{1}{2}u^3)+\frac{\partial}{\partial z}(\tfrac{1}{2}u^2w)=-Rgu\frac{\partial}{\partial x}\int_z^\infty c\,\mathrm{d}z+\frac{\partial}{\partial z}(u\tau)+RgcuS-\tau\frac{\partial u}{\partial z}. \tag{A 20}$$

The equation of mean energy balance of the turbulence, (A 12), approximates to

$$\frac{\partial k}{\partial t}+\frac{\partial uk}{\partial x}+\frac{\partial wk}{\partial z}=\tau\frac{\partial u}{\partial z}-\frac{\partial}{\partial z}\overline{\left[w'\left(\frac{p'}{\rho}+\tfrac{1}{2}u_i'u_i'\right)\right]}-\epsilon-RgF, \tag{A 21}$$

where

$$\epsilon=\nu\overline{\frac{\partial u_i'}{\partial x_j}\frac{\partial u_i'}{\partial x_j}}. \tag{A 22}$$

The parameter ϵ denotes the mean dissipation rate per unit mass of fluid due to the turbulence.

The sediment in the turbidity current affects the energy balance in three important ways. The work done on the sediment by gravity yields the source of power for the flow in the form of the term $RgcuS$ in (A 20). On the other hand, kinetic energy is lost to the flow by the work of turbulence against the downward normal density gradient, represented by the term RgF in (A 21). Finally, down-channel changes in mean concentration yield a work term associated with changing pressure, the term $-Rgu(\partial/\partial x)\int_z^\infty c\,\mathrm{d}z$ in (A 20).

The term representing the work of turbulence against the density gradient can be further reduced with the aid of (A 18), which after some manipulation integrates to yield

$$F=v_s c+\frac{\partial}{\partial t}\int_z^\infty c\,\mathrm{d}z+\frac{\partial}{\partial x}\int_z^\infty uc\,\mathrm{d}z-wc. \tag{A 23}$$

Using (A 14) to eliminate w, then, (A 21) becomes

$$\frac{\partial k}{\partial t}+\frac{\partial uk}{\partial x}+\frac{\partial wk}{\partial z}=\tau\frac{\partial u}{\partial z}-\frac{\partial}{\partial z}\overline{\left[w'\left(\frac{p'}{\rho}+\tfrac{1}{2}u_i'u_i'\right)\right]}-\epsilon-Rgv_s c$$
$$-Rg\left[\frac{\partial}{\partial t}\int_z^\infty c\,\mathrm{d}z+\frac{\partial}{\partial x}\int_z^\infty uc\,\mathrm{d}z+c\frac{\partial}{\partial x}\int_0^z u\,\mathrm{d}z\right]. \tag{A 24}$$

A.3. *Vertically integrated balance equations*

For the geometry of figure 1, (A 16), (A 20) and (A 24) can be integrated in the z-direction to yield the following relations: mean momentum balance

$$\frac{\partial}{\partial t}\int_0^\infty u\,\mathrm{d}z+\frac{\partial}{\partial x}\int_0^\infty u^2\,\mathrm{d}z=-Rg\frac{\partial}{\partial x}\int_0^\infty\int_z^\infty c\,\mathrm{d}z'\,\mathrm{d}z+RgS\int_0^\infty c\,\mathrm{d}z-u_*^2, \quad \text{(A 25)}$$

where

$$u_*^2=\tau|_{z=b}=-\overline{u'w'}|_{z=b} \quad \text{(A 26)}$$

denotes an approximation of the kinematic bed shear stress $\tau|_{z=0}$, and $z=b$ denotes a level very close to the bed but outside any range where viscous effects are important; energy balance of the mean flow

$$\frac{\partial}{\partial t}\int_0^\infty \tfrac{1}{2}u^2\,\mathrm{d}z+\frac{\partial}{\partial x}\int_0^\infty \tfrac{1}{2}u^3\,\mathrm{d}z=-Rg\int_0^\infty u\frac{\partial}{\partial x}\int_z^\infty c\,\mathrm{d}z'\,\mathrm{d}z+RgS\int_0^\infty cu\,\mathrm{d}z-P_{\mathrm{T}}, \quad \text{(A 27)}$$

where

$$P_{\mathrm{T}}=\int_0^\infty \tau\frac{\partial u}{\partial z}\mathrm{d}z \quad \text{(A 28)}$$

denotes the integrated mean rate of transfer of kinetic energy from the mean flow to the turbulence; and the mean energy balance of the turbulence

$$\frac{\partial}{\partial t}\int_0^\infty k\,\mathrm{d}z+\frac{\partial}{\partial x}\int_0^\infty uk\,\mathrm{d}z=P_{\mathrm{T}}-\int_0^\infty \epsilon\,\mathrm{d}z-Rgv_{\mathrm{s}}\int_0^\infty c\,\mathrm{d}z$$
$$-Rg\left[\frac{\partial}{\partial t}\int_0^\infty\int_z^\infty c\,\mathrm{d}z'\,\mathrm{d}z+\frac{\partial}{\partial x}\int_0^\infty\int_z^\infty uc\,\mathrm{d}z'\,\mathrm{d}z+\int_0^\infty c\frac{\partial}{\partial x}\int_0^z u\,\mathrm{d}z'\,\mathrm{d}z\right]. \quad \text{(A 29)}$$

The equation of mean fluid mass balance, (A 14), integrates to yield

$$\frac{\partial}{\partial x}\int_0^\infty u\,\mathrm{d}z+w_\infty=0, \quad \text{(A 30)}$$

where w_∞ is a fictitious velocity necessitated by the nature of the boundary-layer approximations. For boundary layers of the type of figure 1, it is customary to set

$$w_\infty=\frac{\partial h}{\partial t}-w_{\mathrm{e}},$$

where $\partial h/\partial t$ represents the temporal rate of growth of the thickness h of the boundary layer, and w_{e} is an entrainment velocity. Thus (A 30) becomes

$$\frac{\partial h}{\partial t}+\frac{\partial}{\partial x}\int_0^\infty u\,\mathrm{d}z=w_{\mathrm{e}}. \quad \text{(A 31)}$$

The thickness of the boundary layer h is defined below.

The equation of mean sediment mass balance, (A 18), integrates to yield

$$\frac{\partial}{\partial t}\int_0^\infty c\,\mathrm{d}z+\frac{\partial}{\partial x}\int_0^\infty uc\,\mathrm{d}z=F_{\mathrm{b}}-v_{\mathrm{s}}c_{\mathrm{b}}, \quad \text{(A 32)}$$

where

$$F_{\mathrm{b}}=F|_{z=b}=\overline{c'w'}|_{z=b};\quad c_{\mathrm{b}}=c|_{z=b}. \quad \text{(A 33)}$$

Again, the vertical-flux terms have been evaluated slightly above the bed in order to avoid singular behaviour associated with the neglect of the molecular diffusivity. However no matter how h is defined, it is clear that the condition $b/h \ll 1$ must be satisfied in order to justify the approximation inherent in (A 25) and (A 32).

The term F_b represents the rate of entrainment of sediment from the bed into the suspension by turbulence. A dimensionless entrainment rate E_s can be defined such that $F_b = v_s E_s$, so (A 32) takes the form

$$\frac{\partial}{\partial t}\int_0^\infty c\,dz + \frac{\partial}{\partial x}\int_0^\infty uc\,dz = v_s(E_s - c_b). \tag{A 34}$$

Equation (A 34) quantifies the change in the amount of sediment in suspension in terms of net down-valley inflow and outflow, and net gain by entrainment from (or loss by deposition to) the bed.

A.4. *Similarity assumptions: the slab approximations*

From this point on, it is necessary to make several rather severe assumptions in order to allow for a tractable model. The first is the assumption of similarity. The parameters u, c and k are assumed to maintain approximately similar profiles in the z-direction as they change in time or in the down-valley direction, that is, it is assumed that

$$u(x,z,t) = U(x,t)\,\zeta_u(\eta), \tag{A 35a}$$

$$c(x,z,t) = C(x,t)\,\zeta_c(\eta), \tag{A 35b}$$

$$k(x,z,t) = K(x,t)\,\zeta_k(\eta), \tag{A 35c}$$

where

$$\eta = \frac{z}{h(x,t)}$$

and ζ_u, ζ_c and ζ_k are approximated to be functions of η alone. The layer-averaged quantities U, C and K, and also the layer thickness h, can be determined via four appropriately defined moments. One example of such a set of moments is

$$Uh = \int_0^\infty u\,dz \quad \left(\int_0^\infty \zeta_u\,d\eta = 1\right), \tag{A 36a}$$

$$UKh = \int_0^\infty uk\,dz \quad \left(\int_0^\infty \zeta_u\zeta_k\,d\eta = 1\right), \tag{A 36b}$$

$$UCh = \int_0^\infty uc\,dz \quad \left(\int_0^\infty \zeta_u\zeta_c\,d\eta = 1\right), \tag{A 36c}$$

$$U^2h = \int_0^\infty u^2\,dz \quad \left(\int_0^\infty \zeta_u^2\,d\eta = 1\right) \tag{A 36d}$$

(see e.g. Ellison & Turner 1959). Herein K is referred to as the 'level of turbulence'.

The following relations are obtained with the aid of (A 35*a–c*) and (A 36*a–d*): the equation of fluid mass balance, from (A 31),

$$\frac{\partial h}{\partial t} + \frac{\partial Uh}{\partial x} = w_e; \tag{A 37}$$

the equation of sediment mass balance, from (A 34),

$$\left[\int_0^\infty \zeta_c\,d\eta\right]\frac{\partial Ch}{\partial t} + \frac{\partial UCh}{\partial x} = v_s(E_s - c_b); \tag{A 38}$$

the equation of momentum balance, from (A 25),

$$\frac{\partial Uh}{\partial t} + \frac{\partial U^2h}{\partial x} = -\left[\int_0^\infty\int_\eta^\infty \zeta_c\,d\eta'\,d\eta\right]Rg\frac{\partial Ch^2}{\partial x} + \left[\int_0^\infty \zeta_c\,d\eta\right]RgChS - u_*^2; \tag{A 39}$$

the equation of energy balance of the mean flow, from (A 27),

$$\frac{\partial}{\partial t}\frac{1}{2}U^2h+\left[\int_0^\infty \zeta_u^3\,\mathrm{d}\eta\right]\frac{\partial}{\partial x}\frac{1}{2}U^3h = RgChUS-Ph$$
$$-\left[\int_0^\infty \zeta_u\int_\eta^\infty \zeta_c\,\mathrm{d}\eta'\,\mathrm{d}\eta\right]RgU\frac{\partial Ch^2}{\partial x}-\left[\int_0^\infty \eta\frac{\mathrm{d}\zeta_u}{\mathrm{d}\eta}\int_\eta^\infty \zeta_c\,\mathrm{d}\eta'\,\mathrm{d}\eta\right]RghUC\frac{\partial h}{\partial x}; \quad \text{(A 40)}$$

and the equation of mean energy of the turbulence, from (A 29),

$$\left[\int_0^\infty \zeta_k\,\mathrm{d}\eta\right]\frac{\partial Kh}{\partial t}+\frac{\partial UKh}{\partial x} = (P-\epsilon_0)h-\left[\int_0^\infty \zeta_c\,\mathrm{d}\eta\right]Rgv_sCh$$
$$-Rg\left\{\left[\int_0^\infty\int_\eta^\infty \zeta_c\,\mathrm{d}\eta'\,\mathrm{d}\eta\right]\frac{\partial Ch^2}{\partial t}+\left[\int_0^\infty\int_\eta^\infty \zeta_u\zeta_c\,\mathrm{d}\eta'\,\mathrm{d}\eta\right]\frac{\partial UCh^2}{\partial x}\right.$$
$$\left.+\left[\int_0^\infty \zeta_c\int_0^\eta \zeta_u\,\mathrm{d}\eta'\,\mathrm{d}\eta\right]hC\frac{\partial Uh}{\partial x}-\left[\int_0^\infty \eta\,\zeta_c\zeta_u\,\mathrm{d}\eta\right]ChU\frac{\partial h}{\partial x}\right\}, \quad \text{(A 41)}$$

where
$$\epsilon_0 h=\int_0^\infty \epsilon\,\mathrm{d}z; \quad P=P_T/h.$$

Equations (A 38)–(A 41) contain numerous shape factors that cannot be evaluated in the absence of experimental data, but can nevertheless be expected to be of order unity. Some assumption is needed concerning them if further progress is to be made. The simplest one is that called the 'top-hat' assumption by Turner (1973, p. 168), or the 'slab' assumption by Pantin (1979):

$$\zeta_u(\eta)=\zeta_c(\eta)=\zeta_k(\eta)=\begin{cases}1 & \text{for } 0\leqslant\eta\leqslant 1,\\ 0 & \text{for } \eta>1,\end{cases} \quad \text{(A 42)}$$

With (A 42), equations (A 38), (A 39) and (A 40) reduce to

$$\frac{\partial Ch}{\partial t}+\frac{\partial UCh}{\partial x}=v_s(E_s-c_b), \quad \text{(A 43)}$$

$$\frac{\partial Uh}{\partial t}+\frac{\partial U^2h}{\partial x}=-\tfrac{1}{2}Rg\frac{\partial Ch^2}{\partial x}+RgChS-u_*^2, \quad \text{(A 44)}$$

$$\frac{\partial}{\partial t}\frac{1}{2}U^2h+\frac{\partial}{\partial x}\frac{1}{2}U^3h=RgChUS-Ph-\tfrac{1}{2}RgU\frac{\partial Ch^2}{\partial x}. \quad \text{(A 45)}$$

Equations (A 42), (A 37) and (A 43) allow (A 41) to be reduced to

$$\frac{\partial Kh}{\partial t}+\frac{\partial UKh}{\partial x}=(P-\epsilon_0)h-Rgv_sCh-\tfrac{1}{2}RgChw_e-\tfrac{1}{2}Rghv_s(E_s-c_b). \quad \text{(A 46)}$$

It is apparent from (A 37), (A 44) and (A 45) that u_*, w_e and P cannot be specified independently; if (A 44) is multiplied by U and reduced with (A 37), the result is

$$\frac{\partial}{\partial t}\frac{1}{2}U^2h+\frac{\partial}{\partial x}\frac{1}{2}U^3h=RgChUS-\tfrac{1}{2}w_eU^2-u_*^2U-\tfrac{1}{2}RgU\frac{\partial Ch^2}{\partial x}. \quad \text{(A 47)}$$

Comparing (A 47) and (A 45), it is seen that

$$Ph=u_*^2U+\tfrac{1}{2}U^2w_e. \quad \text{(A 48)}$$

The result is accurate only for shape factors expected to be close to unity.

Recently Garcia (1985) utilized data from experiments on turbidity currents to evaluate the similarity hypotheses embodied in (A 35*a*) and (A 35*b*), and the shape

factors involving velocity and concentration appearing in (A 38), (A 39), (A 40) and (A 41). Within the range of the experiments, similarity was shown to be approximated well. Those shape factors that could be evaluated varied from 38 % less than to 13 % greater than the values yielded by the top-hat assumption. The top-hat assumption was found to yield good approximations of the shape factors in nearly all cases.

REFERENCES

Akiyama, J. & Fukushima, Y. 1985 Entrainment of noncohesive bed sediment into suspension. *External Memo.* No. 175, St. Anthony Falls Hydraulic Laboratory, University of Minnesota, Minneapolis, USA.

Bagnold, R. A. 1962 Auto-suspension of transported sediment, turbidity currents. *Proc. R. Soc. Lond.* A **265**, 315–319.

Chu, F. H., Pilkey, W. D. & Pilkey, O. H. 1979 An analytical study of turbidity current steady flow. *Mar. Geol.* **33**, 205–220.

Egashira, S. 1980 Basic research on the flow and mechanism of mixing of density-stratified fields. Ph.D. thesis, Kyoto University, Japan.

Ellison, T. H. & Turner, J. S. 1959 Turbulent entrainment in stratified flows. *J. Fluid Mech.* **6**, 423–448.

Fukushima, Y., Parker, G. & Pantin, H. M. 1985 Prediction of ignitive turbidity currents in Scripps Submarine Canyon. *Mar. Geol.* **67**, 55–81.

Garcia, M. H. 1985 Experimental study of turbidity currents. M.S. thesis, Dept. of Civil and Mineral Engineering, University of Minnesota, USA.

Gartshore, I. S. & Newman, B. G. 1969 The turbulent wall jet in an arbitrary pressure gradient. *Aeronaut. Q.* **20**, 25–56.

Henderson-Sellers, B. 1981 Shape constants for plume models. *Bound.-Layer Met.* **21**, 105–114.

Hinze, J. O. 1960 On the hydrodynamics of turbidity currents. *Geol. Mijnb.* **39e**, 18–25.

Inman, D. L., Nordstrom, C. E. & Flick, R. E. 1976 Currents in submarine canyons: an air–sea–land interaction. *Ann. Rev. Fluid Mech.* **8**, 275–310.

Knapp, R. T. 1938 Energy balance in streams carrying suspended load. *Trans. A.G.U.* **1**, 501–505.

Komar, P. D. 1977 Computer simulation of turbidity current flow and the study of deep-sea channels and fan sedimentation. In *The Sea: Ideas and Observations on Progress in the Study of the Sea*, Vol. 6, Chap. 15 (ed. E. D. Goldberg, I. N. McCave, J. J. O'Brien & J. H. Steele), pp. 603–621. Wiley.

Krause, D. C., White, W. C., Piper, D. J. W. & Heezen, B. C. 1970 Turbidity currents and cable breaks in the western New Britain Trench. *Bull. Geol. Soc. Am.* **81**, 2153–2160.

Launder, B. E. & Spalding, D. B. 1972 *Mathematical Models of Turbulence.* Academic.

Longuet-Higgins, M. S. & Turner, J. S. 1974 An 'entraining plume' model of a spilling breaker. *J. Fluid Mech.* **63**, 1–20.

Lüthi, S. 1981 Some new aspects of two-dimensional turbidity currents. *Sedimentology* **28**, 97–105.

Mathieu, J. & Tailland, A. 1965 Jet pariétal. *C. R. Acad. Sci. Paris* **261**, 2282–2285.

Michon, X., Goddet, J. & Bonnefille, R. 1955 *Etude Théorique et Expérimentale des Courants de Densité.* Tomes I, II, Lab. Natl Hydraulique, Chatou, France.

Myers, G. E., Schauer, J. J. & Eustis, R. H. 1961 The plane turbulent wall jet. 1. Jet development and friction factor. *Tech. Rep.* No. 1, Dept of Mech. Engng, Stanford University.

Pantin, H. M. 1979 Interaction between velocity and effective density in turbidity flow: phase-plane analysis, with criteria for autosuspension. *Mar. Geol.* **31**, 59–99.

Parker, G. 1978 Self-formed straight rivers with equilibrium banks and mobile bed. Part 1. The sand-silt river. *J. Fluid Mech.* **89**, 109–125.

Parker, G. 1982 Conditions for the ignition of catastrophically erosive turbidity currents. *Mar. Geol.* **46**, 307–327.

PLAPP, J. E. & MITCHELL, J. P. 1960 A hydrodynamic theory of turbidity currents. *J. Geophys. Res.* **65**, 983–992.

RAJARATNAM, N. 1976 *Turbulent Jets*. Elsevier.

SCHWARZ, W. H. & COSART, W. P. 1961 The two-dimensional wall jet. *J. Fluid Mech.* **10**, 481–495.

SIGALLA, A. 1958 Measurements of skin friction in a plane turbulent wall jet. *J. R. Aeronaut. Soc.* **62**, 873–877.

TESAKER, E. 1969 Uniform turbidity currents. Thesis in Civil Engineering, Tech. Univ. Norway.

SHEPARD, F. P. & DILL, R. F. 1966 *Submarine Canyons and Other Sea Valleys*. Rand McNally.

TURNER, J. S. 1973 *Buoyancy Effects in Fluids*. Cambridge University Press.